Corrected 15 October 2020; see below

science.sciencemag.org/cgi/content/full/science.abd6176/DC1

Supplementary Materials for

Microbiota-modulated CART enteric neurons autonomously regulate blood glucose

Paul A. Muller*†, Fanny Matheis*, Marc Schneeberger*, Zachary Kerner, Veronica Jové, Daniel Mucida†

*These authors contributed equally to this work.
†Corresponding author. Email: pmuller@rockefeller.edu (P.A.M.); mucida@rockefeller.edu (D.M.)

Published 27 August 2020 on *Science* First Release
DOI: 10.1126/science.abd6176

This PDF file includes:

Other Supporting Online Material for this manuscript includes the following:
(available at science.sciencemag.org/cgi/content/full/science.abd6176/DC1)

MDAR Reproducibility Checklist (.pdf)
Movies S1 to S5 (.mov)

Correction: Figure S15 was added. Our final mouse experiments were substantially affected by Rockefeller coronavirus disease 2019 (COVID-19) lab closures, and thus we acknowledge that our initial sample sizes for *Snap25*$^{\Delta Casp11}$ were below the standard for an animal experiment, despite two independent experiments having been run. In the time between the First Release and print publication, we were able to complete a final antibiotic treatment experiment in *Snap25*$^{\Delta Casp11}$ mice. We present these findings with increased *n* in fig. S15.

Materials and Methods

Mice. Wild-type mice used: C57BL/6J (C57BL/6J, Jackson, 000664 or C57BL/6NTac, Taconic, B6-M/F). Transgenic mice used: RiboTag (B6N.129-*Rpl22*$^{tm1.1Psam}$, Jackson, 011029), *Snap25*^{Cre} (B6;129S-*Snap25*$^{tm2.1(cre)Hze}$, Jackson, 023525), *Cart*^{Cre} (B6;129S-Cartpttm1.1(cre)Hze/J, Jackson, 028533), *Npy*^{Cre} (B6.Cg-Npytm1(cre)Zman/J, Jackson, 027851), *Agrp*^{Cre} (Agrptm1(cre)Lowl/J, Jackson, 012899), *Rosa26*$^{lsl\text{-}tdTomato}$ (B6.Cg-*Gt(ROSA)26Sor*$^{tm14(CAG\text{-}tdTomato)Hze}$, Jackson, 007914), *Casp1*$^{-/-}$ *Casp11*$^{-/-}$(B6N.129S2-Casp1tm1Flv/J, Jackson, 016621), *Casp11*$^{-/-}$ (Casp4tm1Yuan/J, Jackson, 024698) *Nlrp6*$^{flox/flox}$ by P. Rosenstiel (targeting of Exon 1 of *Nlrp6*, frozen sperm generously provided by T. Kanneganti), and *Casp11*$^{flox/flox}$ by KOMP and A. Wullaert. Gnotobiotic mice used: Germ-Free (GF) C57BL/6J and *Snap25*^{RiboTag}. For comparisons to GF mice, respective SPF mice were maintained on sterilized Autoclavable Mouse Breeder Diet (5021, LabDiet, USA) (GF diet), the same used in the gnotobiotic facility. Controls for GF C57BL6/J mice were previously GF and kept on a GF diet under SPF conditions for several generations (exGF). Controls for GF *Snap25*^{RiboTag} mice were *Snap25*^{RiboTag} SPF mice maintained on a GF diet. All other mice used in this study were maintained on a standard Mouse Breeder Diet and we note no difference in fasting blood glucose levels between mice fed a standard diet and those that were switched to a GF diet. ExGF and all other WT or transgenic mice were housed in the same room in our animal facility under SPF conditions. Housing related to GF colonization with bacteria is detailed below. Mice were bred within our facility to obtain strains described and were 7-12 weeks of age for all experiments unless otherwise indicated. Female mice were used for all sequencing experiments. Male and female mice were used for all other experiments due to multiple genetic models utilized. Estrous cycle was not controlled for in female mice. Animal care and experimentation were consistent with NIH guidelines and approved by the Institutional Animal Care and Use Committee (IACUC) at The Rockefeller University.

Antibiotic treatments. *Chronic combined broad-spectrum antibiotic treatment* (designated "Abx" in figure legends). For chronic microbial depletion, 0.25 g vancomycin (Sigma, V2002), 0.25 g metronidazole (Sigma, M3761), 0.5 g ampicillin (Sigma, A0166) and 0.5 g neomycin (Sigma, N6386) were dissolved in 500 mL of filtered water supplemented with 5 g Splenda® to control for the bitter taste of the antibiotic solution. Splenda controls were given filtered drinking water supplemented with 10 g^{-L} of Splenda. Body weight was monitored in all mice and analysis was performed at a minimum of 1 week after starting treatment, and only if weights were comparable between relevant groups. All solutions were passed through a SteriCup 0.22 µm filter prior to administration. *Chronic individual antibiotic treatment.* Individual antibiotics (0.25 g vancomycin, 0.25 g metronidazole, 0.5g ampicillin or 0.5 g neomycin) were dissolved in 500 mL of filtered water supplemented with 5 g Splenda. Controls were given filtered drinking water supplemented with 10 g^{-L} of Splenda. *Acute single antibiotic treatment.* For acute microbial depletion, streptomycin (MP Biomedicals, S9137) was prepared in sterile DPBS at a concentration of 200 mg^{-mL} and then filtered with a 0.22 µm (EMD Millipore PES Express) syringe filter. A dose of 20 mg was administered as an oral gavage of 100 µL of this stock solution. Controls received a single gavage of 100 µL sterile DPBS. Mice were analyzed 24 hours or 7 days following this single treatment. *Intraperitoneal antibiotic treatment.* Ampicillin was prepared in sterile DPBS and then filtered with a 0.22 µm (EMD Millipore PES Express) syringe filter. Mice were injected i.p. with either 1 g^{-kg} of Ampicillin or sterile DPBS for 7 days. To control for the stress caused by injections, mice were habituated by mock i.p. injections for at least 5 consecutive days prior to treatment.

Fasting experiments. Unless specified otherwise in figure legends, mice were fasted overnight for 16 hours.

Guanethidine treatment. Guanethidine monosulfate (Sigma, 1301801) was given at 30 mg^{-kg} in combination with 1 mg^{-kg} C21. Blood glucose was then measured at relevant timepoints. To control for stress caused by injections, mice were habituated to mock i.p. injections for at least 5 consecutive days prior to treatment.

CART peptide treatment. CART peptide 55-102 (25 μg^{-kg}, Phoenix Pharmaceuticals, 003-62) was dissolved in sterile 0.9 % sterile saline and aliquots were stored at -20 °C. CART peptide or saline was injected i.p. into mice that were previously treated with broad-spectrum antibiotics for at least 2 weeks. Blood glucose levels were measured 1-hour post-injection. To control for stress caused by injections, mice were habituated to mock i.p. injections for at least 5 consecutive days prior to treatment.

Exendin-9-39 treatment. Exendin-9-39 (Sigma, E7269) was dissolved in 0.9 % sterile saline and aliquots were stored at -20 °C. Exendin-9-39 (40 μg^{-kg}) or saline was administered by i.p. injection to mice previously treated with broad-spectrum antibiotics for at least 2 weeks. Blood glucose were then measured at indicated timepoints. To control for stress caused by injections, mice were habituated to mock i.p. injections for at least 5 consecutive days prior to treatment.

Colonization of germ-free mice. For exGF and *Casp11*$^{-/-}$ colonization experiments measuring fasting blood glucose and intestinal tissue analysis only, GF mice were moved into an SPF room and were housed in a cage with age and sex-matched feces from either exGF or *Casp11*$^{-/-}$ mice kept on an autoclaved germ-free diet. Fasting blood glucose levels from exGF or *Casp11*$^{-/-}$ donor mice were measured to provide a reference point for potential rescue of GF mice. For C57BL/6J colonization experiments measuring fasting blood glucose and gluconeogenesis, male and female GF mice were moved into Tecniplast isolator cages (ISOcages) in a separate room. Age-matched male and female C57BL/6J mice purchased from Jackson Laboratories were also housed in ISOcages in the same room. Following one week of acclimatization, half of the GF mice were then given age and sex-matched feces from C57BL/6J mice. All mice were maintained on autoclaved water and GF diet. All analyses were performed a minimum of two weeks post-conventionalization.

Colonization with antibiotic-resistant flora. During the course of chronic antibiotic treatment, antibiotic-resistant bacteria were detected in the feces of *Casp11*$^{-/-}$ but not C57BL/6J mice. To normalize the microbiota, cages and bedding of the respective experimental groups were regularly switched over the course of antibiotic treatment prior to analysis. Successful colonization with antibiotic-resistant bacteria was determined by bacterial 16S rRNA qPCR of fecal samples and by plating fecal samples on agar plates containing antibiotics. To ensure stable colonization and exclude any effects of the detected antibiotic-resistant bacteria, metabolic and intestinal tissue analyses were performed at least one week after successful colonization was determined.

Virus. The following viruses were used: AAV9-hSyn-DIO-hM3D(Gq)-mCherry (Addgene, 44361), AAV9-hSyn-DIO-hM4Di(Gi)-mCherry (Addgene, 44362), AAV9-hSyn-DIO-mCherry (Addgene, 50459), AAVrg-CAG-FLEX-tdTomato (Addgene, 28306), AAV5-mCherry-FLEX-DTA (UNC Vector Core), AAV5-hSyn-hChR2(H134R)-EYFP (UNC Vector Core), and PRV-152/614 (Gift of L. Enquist). Fast Green (Sigma, F7252) was added (0.1%) to virus injected into peripheral tissues.

Viral injections. Mice were anesthetized with 2% isoflurane with 1% oxygen followed by 1% isoflurane with 1% oxygen to maintain anesthesia. After shaving and sterilization of the abdomen, mice were placed on a sterile surgical pad on top of a heating pad and covered with a sterile surgical drape. Ophthalmic ointment was placed over the eyes to prevent dehydration and the incision site was sterilized. Upon loss of recoil paw compression, a midline incision was made through the abdominal wall exposing the peritoneal cavity. The duodenum, ileum, colon, or CG-SMG were located and exposed for injection. All injections were made with a pulled glass pipette using a Nanoject III. The following volumes were used for each viral injection into a different region of the intestine: AAVrg-CAG-tdTomato (1.25 µL), AAV9-hSyn-DIO-hM3D(Gq)-mCherry (1.25 µL), AAV9-hSyn-DIO-hM4D(Gi)-mCherry (1.25 µL), AAV9-hSyn-DIO-mCherry (1.25 µL), AAV5-mCherry-FLEX-DTA (2.5 µL), and AAV5-hSyn-hChR2(H134R)-EYFP (2 µL). Following injection, the abdominal wall was closed using

absorbable sutures and the skin was closed using surgical staples. Antibiotic ointment was applied to the closed surgical site and mice were given 0.05 mg^{-kg} buprenorphine every 12 h for 2 days. All mice with viral transduction in the intestine (hM3Dq, hM4Di, mCherry, hChR2, and DTA) were analyzed starting at two weeks post-injection.

Viral strategies. *Cart*^{Cre}*, Agrpt*^{Cre}*, Npy*^{Cre} *anatomical mapping* (*28*). AAVrg-CAG-tdTomato (*26*) was injected into the duodenum, ileum, and colon of *Cart*$^{Cre+}$*, Agrpt*$^{Cre+}$*, Npy*$^{Cre+}$ mice. *Cart*^{Cre} *modulation*. hM3Dq: AAV9-hSyn-DIO-hM3Dq-mCherry (*42*)was injected into the ileum and colon of Cart^{Cre+} mice. Controls were AAV9-hSyn-DIO-hM3Dq-mCherry injected into the ileum and colon of *Cart*$^{Cre–}$ mice or AAV9-hSyn-DIO-mCherry into the ileum and colon of *Cart*$^{Cre+}$ mice. All mice were injected with 1 mg^{-kg} of Compound 21. hM4Di: AAV9-hSyn-DIO-hM4Di-mCherry was injected into the ileum and colon of *Cart*$^{Cre+}$ mice. Mice were injected with 1 mg^{-kg} of Compound 21 or saline (controls). *Cart*^{Cre} *ablation*. AAV5-mCherry-FLEX-DTA (*43*) was injected into the ileum and colon of Cart^{Cre+} mice. Controls were AAV5-hSyn-hChR2(H134R)-EYFP injected into the ileum and colon of *Cart*$^{Cre+}$ mice.

CTB viscerofugal tracing. Mice were anesthetized and operated on as described above. 1.5 µL of 1% CTB-488, -555, or -647 (Thermo Fisher Scientific, C34775, C22843 and C34778) in PBS with 0.1% Fast Green (Sigma, F7252) was injected with a pulled glass pipette using a Nanoject III into the CG-SMG. Relevant tissues were then dissected after a minimum of 2- 4 days post-injection.

Chemogenetics. Water soluble Compound 21 (HelloBio, HB6124) was dissolved in sterile 0.9% saline. Mice were given an intraperitoneal injection at a dose of 1 mg^{-kg} .

cFos counting. Mice were sacrificed by cervical dislocation and CG-SMG were harvested and fixed overnight in 4% PFA/PBS. CG-SMG were then washed four times in DPBS at RT and permeabilized in 0.5% Triton X-100/0.05% Tween-20/4 µg heparin (PTxwH) overnight RT. Primary antibody cFos (1:1000, Cell Signaling Technologies, 2250S) was added to the samples in PTxwH and incubated at 4°C for 72 h. Samples were washed four times in PTxwH at RT and then stained with goat-anti rabbit AF555/568/647 (Thermo Fisher Scientific) (Thermo Fisher Scientific, A11034, A11036 and A21245) at 4°C for 48-72 h. Samples were washed four times in PTxwH at RT, covered in Fluoromount G, and coverslipped for confocal imaging. We captured all sympathetic neurons within the CG-SMG with multiple z-stack images. All images were analyzed in Image-J. Total cFos+ nuclei were counted using the Cell Counter plugin for Image-J, and data were not normalized to area or volume. Each data point represents the number of cFos+ cells per CG-SMG.

Brain immunofluorescence. Mice were sacrificed and transcardially perfused with cold PBS with heparin followed by cold 4% PFA (Electron Microscopy Sciences). The intact brain was separated carefully from the skull and placed in 4% PFA, and then rotated for 48 h at 4°C. Whole brains were washed with PBS/0.03%Azide and sectioned at 50 µm on a Leica vibratome for immunofluorescence. Samples were then permeabilized in 0.5% Triton/0.05% Tween-20 in PBS (PTx) followed by blocking in 5% goat serum in PTxwH each for 2 h at room temperature. Primary antibody was added to the blocking buffer and samples were incubated with constant rotation at 4°C overnight. Four 15-minute washes were done in PTxwH at RT after which samples were moved to blocking buffer with secondary antibody. Slices were incubated in secondary antibody for 2 hours at room temperature followed by four 15-minute washes in PTxwH at room temperature. Samples were then placed on microscope slides, covered in Fluoromount G, and coverslipped.

Antibodies. The following primary antibodies were used, and unless otherwise indicated concentrations apply to all staining techniques: BIII-Tubulin (1:400, Millipore Sigma, T2200; 1:200, Aves Labs, TUJ), NPY (1:200, Immunostar, 22940), SST (1:400, Millipore Sigma, MAB354), RFP (1:1000, Sicgen, AB8181; 1:1000,

Rockland, 600-401-379), pCREB Ser133 (1:200, Cell Signaling Technologies, 9198S), ANNA-1 (1:200,000, Gift of Dr. Vanda A. Lennon), cFos (1:1000, Cell Signaling Technologies, 2250S), HA (1:400, Cell Signaling Technologies, 3724S), CART (1:500, R&D Systems, AF163), CD9 (AF647, 1:200, BD Biosciences, 564233). Fluorophore-conjugated secondary antibodies were either H&L or Fab (Thermo Fisher Scientific) at a consistent concentration of 1:400 in the following species and colors: goat anti-rabbit (AF488/568/647), goat anti-rat (AF488/647), goat anti-chicken (AF488/568/647), goat anti-human (AF488/568/647), donkey anti-guinea pig (AF488/647), donkey anti-rabbit (AF568/647), donkey anti-goat (AF568/647).

Intestine dissection. Mice were sacrificed and duodenum (6 cm moving distal from the gastroduodenal junction), ileum (6 cm moving proximal from the ileocecal junction), or colon (gap of 1 cm from the cecal-colonic junction, then 6 cm moving distal) was removed. For AdipoClear, fecal contents were flushed from the lumen and left intact. For dissection of the *muscularis externa*, following the above procedures, the intestinal tissue was placed on a chilled aluminum block with the serosa facing up. Curved forceps were then used to carefully remove the *muscularis externa* in one intact sheet (*44*).

Nodose ganglion dissection. Mice were sacrificed and the ventral neck surface was cut open. Associated muscle was removed by blunt dissection to expose the trachea and the nodose ganglion (NG) was then located by following the vagus nerve along the carotid artery to the base of the skull. Fine scissors were used to cut the vagus nerve below the NG and superior to the jugular ganglion.

Celiac-superior mesenteric ganglion dissection. Mice were sacrificed and a midline incision was made, and the viscera were reflected out of the peritoneal cavity. The intersection of the descending aorta and left renal artery was identified, from which the superior mesenteric artery was located. The CG-SMG is wrapped around the superior mesenteric artery and associated lymphatic vessels. Fine forceps and scissors were used to remove the CG-SMG.

Dorsal root ganglion dissection. The spinal column was isolated, cleaned of muscle, and bisected sagitally. The spinal cord was removed leaving the dorsal root ganglion (DRG) held in place by the meninges. The thoracic 13 DRG was identified by its position just caudal to thoracic vertebra. The meninges were cleared and the pair of thoracic 9 DRGs were removed with fine forceps and scissors.

RiboTag. Heterozygous or homozygous *Snap25*$^{\text{RiboTag}}$ mice were used for TRAP-seq analysis as no differences were found between either genotype(*3, 4*). For intestine immunoprecipitation (IP), mice were sacrificed, and tissue removed and divided as above. Samples were washed of fecal contents in PBS with cycloheximide (0.2 mg$^{\text{-mL}}$) (PBS/CHX). Mesenteric fat was removed, the *muscularis externa* was separated from the mucosa as described above and samples were washed 5 times in PBS/CHX. For nodose and CG-SMG IP, tissues were isolated as described above. The RiboTag IP protocol was then followed (http://depts.washington.edu/mcklab/RiboTagIPprotocol2014.pdf) with the following modifications. All samples were homogenized by hand with a dounce homogenizer in 2.5 mL supplemented homogenization buffer (changes per 2.5 mL: 50 µL Protease Inhibitor, 75 µL heparin (100 mg$^{\text{-mL}}$ stock), 25 µL SUPERase• In RNase Inhibitor). Samples were then centrifuged for 10 minutes at 10,000 G, after which 800 µL of supernatant was removed and 5µL of anti-HA antibody (Abcam, ab9110) was added. Samples were kept rotating at 4°C with antibody for 1 hour. 200 µL of Thermo Protein magnetic A/G beads were washed with homogenization buffer, added to the sample, and kept rotating for 30 minutes at 4°C. The beads were washed four times with high-salt buffer and samples were eluted with 100 µL of PicoPure lysis buffer. RNA was extracted using the Arcturus PicoPure RNA isolation kit (Applied Biosystems) according to the manufacturer's instructions.

Ribotag RNA-sequencing and differential expression analysis. SMARTer Ultra Low Input RNA (Takara). cDNA libraries were prepared using Nextera XT DNA library preparation kit (Illumina) and sequenced using 75 base-pair single end reads on a NextSeq 500 instrument (Illumina). Reads were aligned using Kallisto to Mouse Ensembl v91 (*5*). Transcript abundance files were imported into RStudio (version 1.3.1; running R version 4.0.2), and DESeq2 (version 1.28.1) (*48*) was used for all downstream differential expression analysis and generation of volcano plots. For intestine samples, Cre+ samples were compared with Cre- samples to generate a list of immunoprecipitated (IP) enriched transcripts (log2FC > 1 and padj < 0.05). A list of total iEAN IP-enriched transcripts was generated by combining all neuronally enriched transcripts from duodenum, ileum, and colon of GF and SPF mice (log2 Fold Change (FC) > 1, padj < 0.05) and was used to perform downstream analyses. All differentially expressed transcripts between samples (gray dots in volcano plots) were then filtered for those contained within the total IP-enriched list (pink dots in volcano plots). Significantly differentially expressed transcripts from each tissue comparison met a cutoff of log2FC > 1, padj < 0.05. PCA plots were generated from log transformed DESeq2 data with the FactoMineR R package (version 2.3). GSEA pre-ranked analysis was performed with desktop software and the C5 gene ontology database using 1000 permutations. Gene ontology enrichment analysis was performed with differentially expressed transcripts (log2FC > 1, padj < 0.05) using the TopGO R package (version 2.40.0) and a Fisher test with an elimination algorithm was used to calculate significance (dashed lines in figures = threshold of significance at 1.3). Duodenum-enriched transcripts were defined as transcripts contained within the total IP enriched list and significantly enriched in the SPF duodenum (log2FC > 1 and padj < 0.05) as compared to both SPF ileum and SPF colon (table S1). We then filtered DESeq2 results for these 86 transcripts in the GF ileum vs SPF ileum and GF colon vs SPF colon comparisons. A duodenum-enriched transcript was considered upregulated in GF tissues if a transcript was significantly enriched (log2FC >1 and padj < 0.05) in the GF sample as compared to the SPF sample.

RiboTag Datasets. GF and SPF duodenum, ileum, and colon *Snap25*$^{\text{RiboTag}}$ TRAP-seq data generated in this manuscript is deposited on the GEO database with accession number GSE156142. SPF nodose, celiac-superior mesenteric, and thoracic 9 dorsal root ganglion *Snap25*$^{\text{RiboTag}}$ TRAP-seq data was previously published (*7*) and is deposited on the GEO database with accession number GSE145986.

TRAP-quantitative real-time PCR. For TRAP-q-RT-PCR, RiboTag-purified mRNA was reverse transcribed using an iScript cDNA Synthesis Kit (BioRad, 1708891) and q-RT-PCR was performed using SYBR green (Bio-Rad Laboratories). The following primers were used: *Rpl32* forward 50-ACAATGTCAAGGAGCTGGAG-30, *Rpl32* reverse 5' – TTGGGATTGGTGACTCTGATG – 3', *Cartpt* forward 5' – TCTACTCTGCCGTGGATGAT – 3', *Cartpt* reverse 5' – CTCTTGAGCTTCTTCAGGACTTC – 3', *Sst* forward 5' – CTGCATCGTCCTGGCTTT – 3', *Sst* reverse GTACTTGGCCAGTTCCTGTT, *Grp* forward TCTCAGTCTCCAGCCTACTT, *Grp* reverse GCAGAGAGTCTACCAACTTAGC, *Nmu* forward AACGGGAAGAGGTCAACAAG, *Nmu* reverse AGGAGGGATCATTTGTGAGAAC. Data were normalized to *Rpl32* (housekeeping gene) and represented as log-transformed expression relative to *Rpl32*.

Fecal DNA extraction. Fecal samples were collected, put on ice following collection and stored at -20 °C until processing. DNA from fecal samples was extracted using a fecal DNA MiniPrep Kit (Zymo Research, D6010) according to the manufacturer's protocol.

Bacterial 16S rRNA qPCR. To monitor germ-free status and luminal bacterial load during antibiotic-mediated microbial depletion and GF colonization experiments, q-RT-PCR was performed on DNA extracted from fecal samples using SYBR green PCR master mix (Applied Biosystems, 43-687-02). The following primers were used to amplify the conserved v3 region of bacterial 16S rRNA: 16S forward 5' – ACTCCTACGGGAGGCAGCAGT– 3' 16S reverse 5' – ATTACCGCGGCTGCTGGC – 3'.

RNAscope whole-mount intestine in-situ hybridization. C57BL/6J, *Cartp*^{Cre}, *Agrp*^{Cre} or *Npy*^{Cre} mice were sacrificed and the duodenum, ileum and colon removed and dissected as described above. Pieces of *muscularis externa* were pinned on Sylgard-coated plates and fixed in 4% PFA at room temperature for 3 hours. Samples were removed from the Sylgard plates and washed in PBS twice for 10 minutes. Samples were further washed twice more in PBS or PBS with 0.1% Tween-20 (PBST) for 10 minutes depending on the origin of the tissue. After washing, pieces of *muscularis externa* were pinned again to Sylgard plates and dehydrated along a gradient of 25/50/75/100/100 % ethanol in PBS or PBST for 10 minutes at each step. 5 mm x 5 mm sections were cut from the tissue and mounted on slides and left to dry (~2 minutes). Samples were digested with 50 µL of protease III digestion solution (ACDbio) at room temperature for between 30 and 45 minutes. After digestion, tissue was removed from slides using forceps and washed three times in PBS for 5 minutes each. Tissue was then hybridized overnight at 40 °C in a humidified oven (ACDbio) using relevant probe targets. Tissue was next amplified and stained according to the RNAScope protocol for whole tissue staining with the following modifications: each amplification step was extended by 5 minutes and following the final amplification samples were washed three times for 10 minutes each. Tissue samples were mounted in Prolong gold antifade with DAPI (Thermo Fisher Scientific) on slides with 1 ½ coverslips. Images were acquired within 24 hours on an inverted LSM 880 NLO laser scanning confocal and multiphoton microscope (Zeiss) and processed using Image J.

Whole-mount intestine immunofluorescence. Following intestine dissection, *muscularis externa* tissue was pinned down on a plate coated with Sylgard, followed by overnight fixation in PBS/4% PFA at 4° C. After washing in DPBS, samples were then permeabilized first in PBS with 0.5% Triton X-100/0.05% Tween-20/(4µg$^{-µL}$) heparin (PTxwH) for 2 hours at room temperature (RT) with gentle agitation. Samples were then blocked for 2 hours in blocking buffer (PTxwH with 5% donkey or goat serum) for 2 hours at RT with gentle agitation. Primary antibodies were added to blocking buffer at appropriate concentrations and incubated for 2-3 days at 4°C. After primary incubation samples were washed in PTxwH, followed by incubation with secondary antibody in PTxwH at appropriate concentrations for 2 hours at RT. Samples were again washed in PTxwH, and then mounted with Fluoromount G on slides with 1 ½ coverslips. Slides were kept in the dark at 4 °C until they were imaged.

Intestine neuronal quantification: total numbers. A minimum of 10 images were randomly acquired across a piece of whole-mount intestine *muscularis externa*. These images were then opened in ImageJ, and the cell counter feature was used to count the number of ANNA-1+ cells in each field. This number was then multiplied by a factor of 3.125 (25x objective, 0.6 zoom), to calculate the number of counted neurons per square millimeter (mm^2). The average of 10 (or more) images were then calculated and plotted. Thus, every point on a given graph corresponds to a single animal. For neuronal subtypes, the number of somatostatin (SST)-, CART-, neuropeptide Y (NPY)- and follistatin (FST)-positive neurons were also counted. These numbers were then reported as both number per mm^2 and as a percentage of ANNA-1+ neurons.

Intestine neuronal quantification: neurons per ganglion. A myenteric ganglion was defined as a continuous group of ANNA-1+ cells that are separated by less than 15 µm in distance. Only complete ganglia were counted per field of view. Thus, the following ganglia were excluded: 1. Ganglia that were truncated; 2. No clear separation (>15 µm) was noted between the last ANNA-1+ cell and the edge of the field of view. In the case of single ANNA-1+ cells that are separated by 15 mm on all sides, this was considered extraganglionic. The number of quantifiable ganglia was averaged across a minimum of 10 images per gut segment per animal.

Feeding assay. Mice were singly housed for at least 5 days prior to beginning the experiment. Before testing mice with Compound 21 (C21), feeding behavior was first assessed with saline injection during the light cycle

(starting at 7:00 AM) and dark cycle (starting at 19:00 PM). Food intake assays were performed in the home cage. Mice were given ad libitum access to food prior to, during, and after the assay. Measurement of food intake (weighing of remaining food at each timepoint) was made at 1, 2, 4, 8, and 24 hours post i.p. injection of C21.

Blood glucose measurement. Mice were fed ad libitum or fasted overnight for 16 hours (indicated in the figure legends) prior to analysis. Mouse tails were cut at the very tip and the first drop of blood was discarded. A single drop of blood was applied to a Breeze2 (Bayer) blood glucose test strip loaded into a Breeze2 blood glucose monitoring system (Bayer). All samples were obtained at the same time of day during the light cycle (10:00-10:30AM).

Intraperitoneal pyruvate tolerance test. Mice were fasted overnight for 16 hours prior to analysis. Mouse tails were cut at the very tip and the first drop of blood was discarded. A single drop of blood was applied to a Breeze2 (Bayer) blood glucose test strip loaded into a Breeze2 blood glucose monitoring system (Bayer). After collecting basal blood glucose, mice were injected at a dose of $1g^{-kg}$ of sodium pyruvate (Sigma, P3662) dissolved in 0.9% in NaCl. Glucose levels were measured after injection at 15, 30, 60, and 120 minutes post-injection to evaluate gluconeogenesis. All samples were obtained at the same time of day during the light cycle (9:00-11 AM).

Blood and plasma collection. Mice were fed ad libitum or fasted overnight for 16 hours (indicated in the figure legends) prior to analysis. Mouse tails were cut at the very tip and the first drop of blood was discarded. At least 100 uL of blood was then collected in a Microvette (Sarsedt Inc., CB300) coated with potassium/EDTA. Tubes were then centrifuged at 3600 RPM for 20 min at 4 °C. Plasma was then collected and frozen at -20°C until analysis. All samples were obtained at the same time of day during the light cycle (10:00-10:30 AM).

Insulin ELISA. Insulin levels in plasma samples were measured using an Ultrasensitive Mouse Insulin ELISA kit (Crystal Chem, 90080) according to the manufacturer's instructions.

Glucagon ELISA. Plasma glucagon concentrations were determined using a Mouse Glucagon ELISA kit (Mercodia, 10-1281-01) according to the manufacturer's protocol.

Retrograde PRV Tracing. Mice were anesthetized and operated as described above. PRV Bartha 152 (GFP) (*49*) or 614 (RFP) (*50*) were a gift of L. Enquist. 3 µL with 0.1% FastGreen was injected with a pulled glass pipette using a Nanoject III into the parenchyma of the right liver lobe or into the head, neck, body, and tail of the pancreas. The intestine *muscularis externa* and CG-SMG were harvested one to four days after injection.

PASTAA analysis. Differentially expressed Ensembl gene ID lists (log2 FC > 1, padj < 0.05) from ileum and colon samples (SPF enriched vs GF) were used in the Predicting Associated Transcription factors from Annotated Affinities (PASTAA) web tool (http://trap.molgen.mpg.de/PASTAA.htm) using default analysis settings and mouse Ensembl 46. Significant (p-value < 0.05) association scores for transcription factors were plotted.

Confocal imaging. Whole-mount intestine, NG, DRG, and CG-SMG samples were imaged on an inverted LSM 880 NLO laser scanning confocal and multiphoton microscope (Zeiss)**.**

AdipoClear. AdipoClear whole tissue clearing was adapted from AdipoClear protocol (*8*). Mice were sacrificed and intestinal sections were removed followed by overnight fixation in 4% PFA. Tissues were washed in PBS then dehydrated in 20/40/60/80/100% Methanol in B1N followed by dichloromethane. Tissues

were then rehydrated in 100/80/60/40/20% methanol in B1N. Subsequently, samples were washed in 0.5% Triton X-100/0.05% Tween-20/(4 µg/µL) heparin (PTxwH) and then incubated in primary antibody dilutions in PTxwH for 7 Days. Samples were washed in PTxwH then incubated in secondary antibody at 1:400 in PTxwH for 7 days. Samples were again washed in PTxwH followed by PBS then dehydrated in 20/40/60/80/100% methanol followed by dichloromethane and finally cleared in dibenzyl ether.

Light-sheet microscopy and 3D reconstruction. Whole-tissue cleared samples were imaged submerged in DBE on a LaVision Biotech Ultramicroscope II with 488 nm, 561 nm or 647 nm light-sheet illumination using a 1.3x or 4x objective with 2.5 µm Z-slices. Images were adjusted post hoc using Imaris x64 software (version 9.1 Bitplane) and 3D reconstructions were recorded as mp4 video files. Optical slices were taken using the orthoslicer or oblique slicer tool.

Intestine motility measurements. For measurement of total intestinal transit time, non-fasted mice were given an oral gavage of 6% carmine red (Sigma, C1022) dissolved in 0.5% methylcellulose (made with sterile 0.9 % saline). Total gastrointestinal transit time (GITT) was measured as the time from oral gavage it took for mice to pass a fecal pellet that contained carmine. Mice in both assays were injected 2 minutes before starting with i.p. Compound 21 (1 mg^{-kg}).

Data replication. All experiments were repeated a minimum of two times. Data points in all graphs are representative of biological replicates.

Statistical analysis. Significance levels indicated are as follows: * $P < 0.05$, ** $P < 0.01$, *** $P < 0.001$ and **** $P < 0.0001$. All data are presented as mean ± s.d.. All statistical tests used were two-tailed. Experiments were not randomized, and no statistical methods were used to predetermine sample size. Investigators were not blinded during experiments or outcome analysis. Multivariate data was analyzed by one-way ANOVA with Tukey's multiple comparisons test, two-way ANOVA with Tukey's multiple comparisons test, or Brown-Forsythe and Welch ANOVA with Dunnett's T3 multiple comparisons test. Comparisons between two conditions were analyzed by unpaired Student's t-test. GraphPad PRISM version 8.2.0 and R 3.4.3 was used for generation of graphs and statistics. For pyruvate tolerance test and Compound 21 treatment, area under the curve (AUC) was measured for each animal with time 0 blood glucose levels set as the baseline. AUC measurements were then compared by two-tailed unpaired t-test.

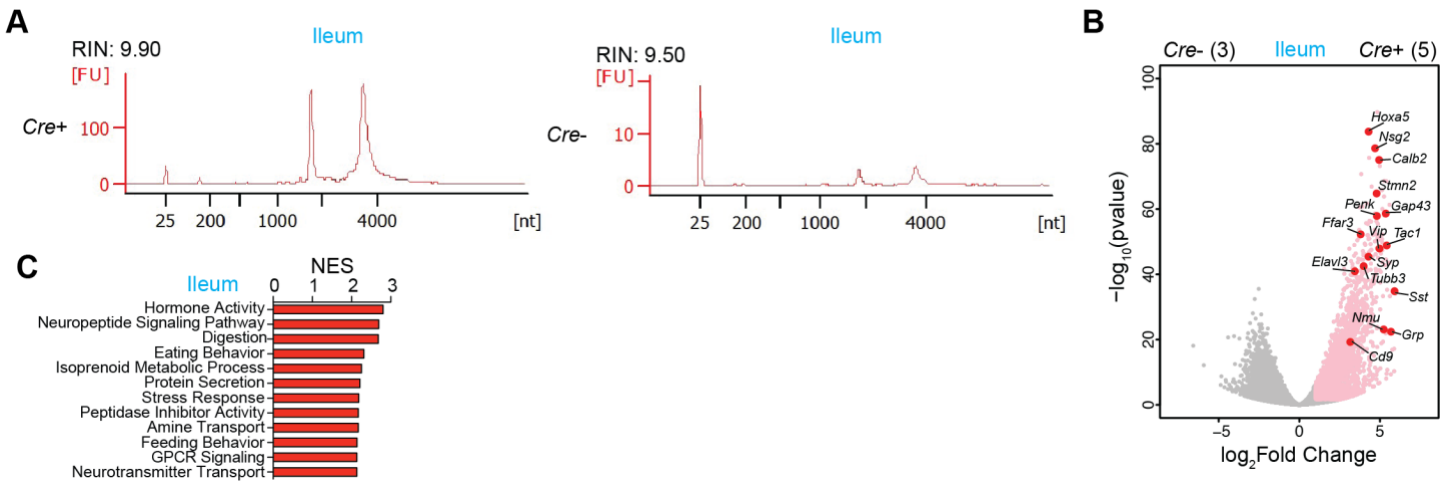

Fig. S1. RiboTag sequencing of myenteric iEAN. (A) Bioanalyzer traces of immunoprecipitated (IP) ribosome-bound mRNA eluted from the ileum *muscularis externa* of *Snap25*^{RiboTag} (Cre+) and *Snap25*$^{Cre–}$ (Cre–) SPF mice. (B) Volcano plot of differentially expressed transcripts between the ileum *muscularis externa* of *Snap25*^{RiboTag} (Cre+) and *Snap25*$^{Cre–}$ (Cre–) SPF mice. Pink dots highlight transcripts with a $\log_2$ Fold Change of >1 and padj-value <0.05. Red dots highlight select IP-enriched transcripts of interest. Number of samples shown in parentheses. (C) Graph of the top 12 gene ontology pathways with a FDR < 25% identified by Gene Set Enrichment Analysis (GSEA) from ileum IP-enriched genes ($\log_2$ Fold Change > 1, padj < 0.05). NES, normalized enrichment score; FDR, false detection rate.

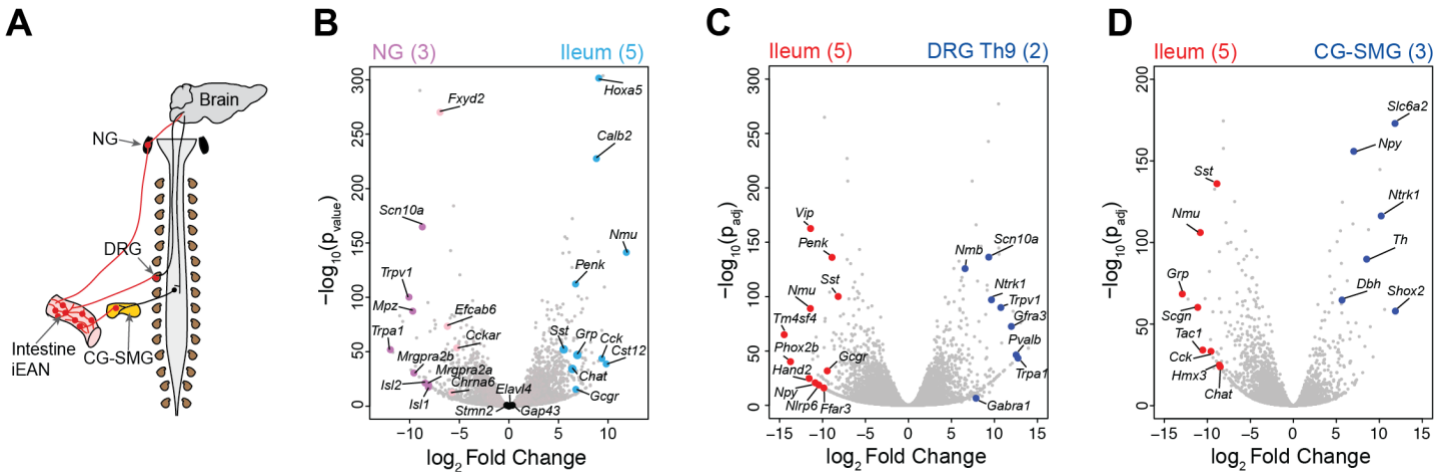

Fig. S2. TRAPseq comparison of ileum iEAN to NG, DRG, and CG-SMG. (A) Anatomical diagram of intrinsic and extrinsic EAN (iEAN and eEAN, respectively). Red dots and lines highlight relevant ganglia and fibers. NG = nodose ganglion, DRG = dorsal root ganglion, CG-SMG = celiac-superior mesenteric ganglion. (B) Volcano plot of differentially expressed transcripts from the nodose ganglion (NG) and ileum myenteric iEAN of *Snap25*^{RiboTag} SPF mice. Grey dots highlight all transcripts analyzed by differential expression analysis. Purple and teal dots highlight differentially expressed transcripts from NG and ileum, respectively. Pink dots highlight ileum IP-enriched transcripts expressed at higher levels in the NG than in the ileum. Black dots highlight neuronal genes that do not significantly differ between samples. Sample numbers are indicated in parentheses. (C) Volcano plot of differentially expressed transcripts compared between the ileum and Th9 DRG of *Snap25*^{RiboTag} SPF mice. Grey dots highlight all transcripts analyzed by differential expression analysis. Red and navy dots highlight transcripts enriched in the ileum and DRG, respectively. Sample numbers are indicated in parentheses. (D) Volcano plot of differentially expressed transcripts compared between the ileum and CG-SMG of *Snap25*^{RiboTag} SPF mice. Grey dots highlight all transcripts analyzed by differential expression analysis. Red and navy dots highlight transcripts enriched in the ileum and CG-SMG, respectively. Sample numbers are indicated in parentheses.

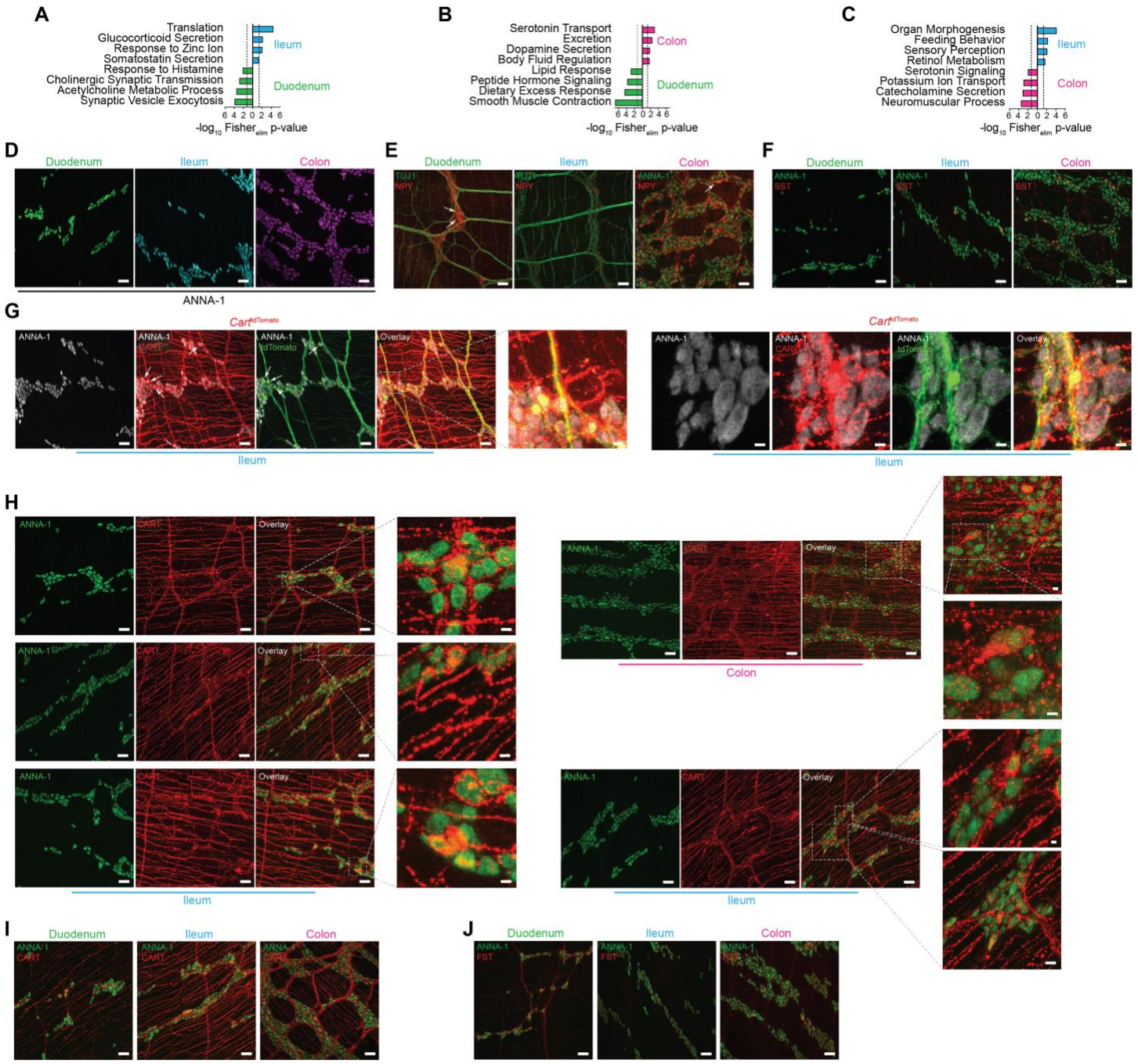

Fig. S3. iEAN anatomical differences in gene pathways and specific genes. (A to C) Gene ontology pathways, identified by TopGO analysis of differentially expressed genes (log_2 Fold Change > 1, padj < 0.05), enriched in (A) the ileum (blue) vs duodenum (green), (B) the colon (magenta) vs duodenum (green), and (C) the ileum (blue) vs colon (magenta) of *Snap25*^{RiboTag} SPF mice. Dashed lines represent threshold of significance (1.3) as calculated by Fisher's test with an elimination algorithm. (D to J) Immunofluorescence whole-mount images of (D) myenteric iEAN (stained with anti-ANNA-1) in the duodenum, ileum, and colon of C57BL/6J SPF mice, (E) NPY+ (red) myenteric iEAN in the duodenum, ileum and colon of C57BL/6J SPF mice, (F) SST+ (red) myenteric iEAN in the duodenum, ileum, and colon of C57BL/6J SPF mice, (G) CART+ (red, stained with antibody) and tdTomato (green, native fluorescence) myenteric iEAN (grey) in the ileum of *Cart*^{tdTomato} SPF mice. White arrows indicate CART+ neurons as determined by staining and reporter. Scale bars (left panel) = 50 µm. Scale bars (inset in middle and right panel) = 10 µm. (H) Different types of CART+ (red) myenteric iEAN (grey) in the ileum and colon of C57BL/6J mice. Scale bars = 50 µm. Scale bars of insets on the right = 10 µm. (I) CART+ (red) myenteric iEAN in the duodenum, ileum, and colon of C57BL/6J SPF mice,

and (J) FST+ (red) myenteric iEAN in the duodenum, ileum, and colon of C57BL/6J SPF mice. Scale bars = 50 μm.

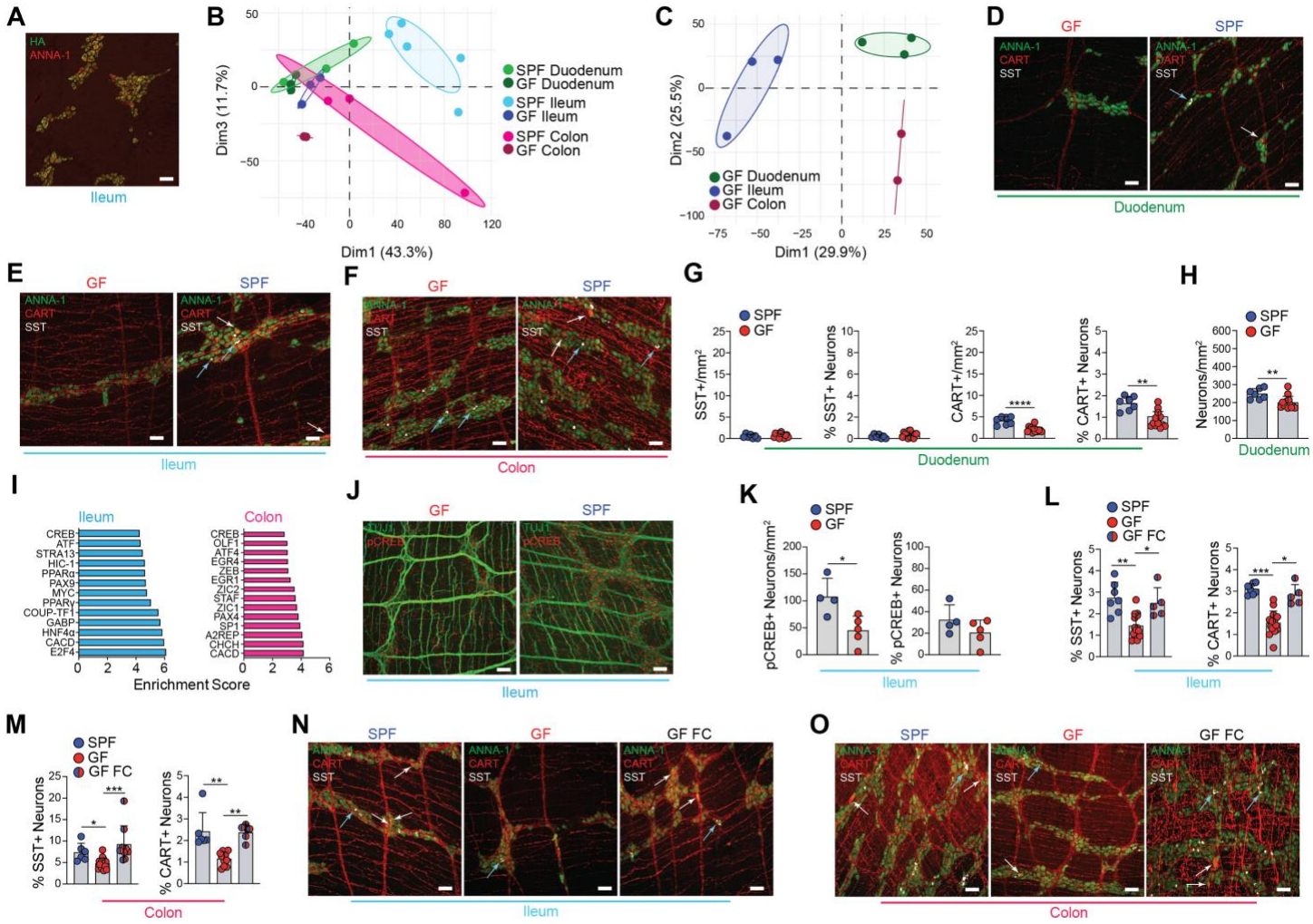

Fig. S4. Microbiota impact the iEAN translatome in a compartmentalized manner. (A) Immunofluorescence staining of the ileum myenteric plexus of *Snap25*^{RiboTag} GF mice using anti-hemagglutinin (HA) and anti-neuronal nuclear (ANNA-1) antibodies. Scale bar = 50 µm. Image representative of ileum myenteric plexus. (B) Principal Component Analysis (PCA) from the duodenum, ileum, and colon iEAN of *Snap25*^{RiboTag} GF and SPF mice. PCA input was filtered for total iEAN IP-enriched transcripts (log_2 Fold Change > 1, padj < 0.05). (C) PCA from the duodenum, ileum, and colon iEAN of *Snap25*^{RiboTag} GF mice. PCA input was filtered for total iEAN IP-enriched transcripts (log_2 Fold Change > 1, padj < 0.05). (D to F) Representative whole-mount IF images of SST+ and CART+ myenteric iEAN in the duodenum (D), ileum (E), and colon (F) of (left) GF and (right) SPF mice. Scale bar = 50 µm. (G) Number and percentage of SST+ (left) and CART+ (right) myenteric iEAN in the duodenum of C57BL/6J GF and SPF mice. ** $P < 0.01$, **** $P < 0.0001$ as calculated by (number) unpaired t-test or (percentage) Mann-Whitney test. (H) Total number of myenteric iEAN in the duodenum of C57BL/6J GF and SPF mice. ** $P < 0.01$ as calculated by unpaired t-test. (I) PASTAA analysis showing enrichment of predicted CREB1 transcription factor binding to the most significant differentially expressed transcripts (log_2 Fold Change > 1, padj < 0.05) of the ileum and colon iEAN between *Snap25*^{RiboTag} GF and SPF mice. (J) Representative confocal immunofluorescent (IF) image of the ileum myenteric plexus of C57BL/6J (left) GF and (right) SPF mice using anti-pCREB (red) and anti-TUJ1 (green) antibodies. Scale bars = 50 µm. (K) Number and percentage of pCREB+ myenteric iEAN in the ileum of C57BL/6J GF and SPF mice. * $P < 0.05$ as calculated by unpaired t-test. (L and M) Percentage of SST+ and CART+ iEAN out of total myenteric iEAN in the ileum (L), and colon (M) of GF, SPF, and GF FC mice. * $P < 0.05$, ** $P < 0.01$, *** $P < 0.001$ as by Kruskal-Wallis test with Dunn's multiple comparisons test. (N and O) Representative whole-mount IF images of SST+ (white) and CART+ (red) myenteric iEAN (green) in the ileum (N) and colon (O) of (left) SPF, (middle) GF, and (right) GF mice colonized with SPF microbiota (fecal

colonization, GF FC). Scale bars = 50 μm. Blue and white arrows point to examples of SST+ and CART+ neurons, respectively.

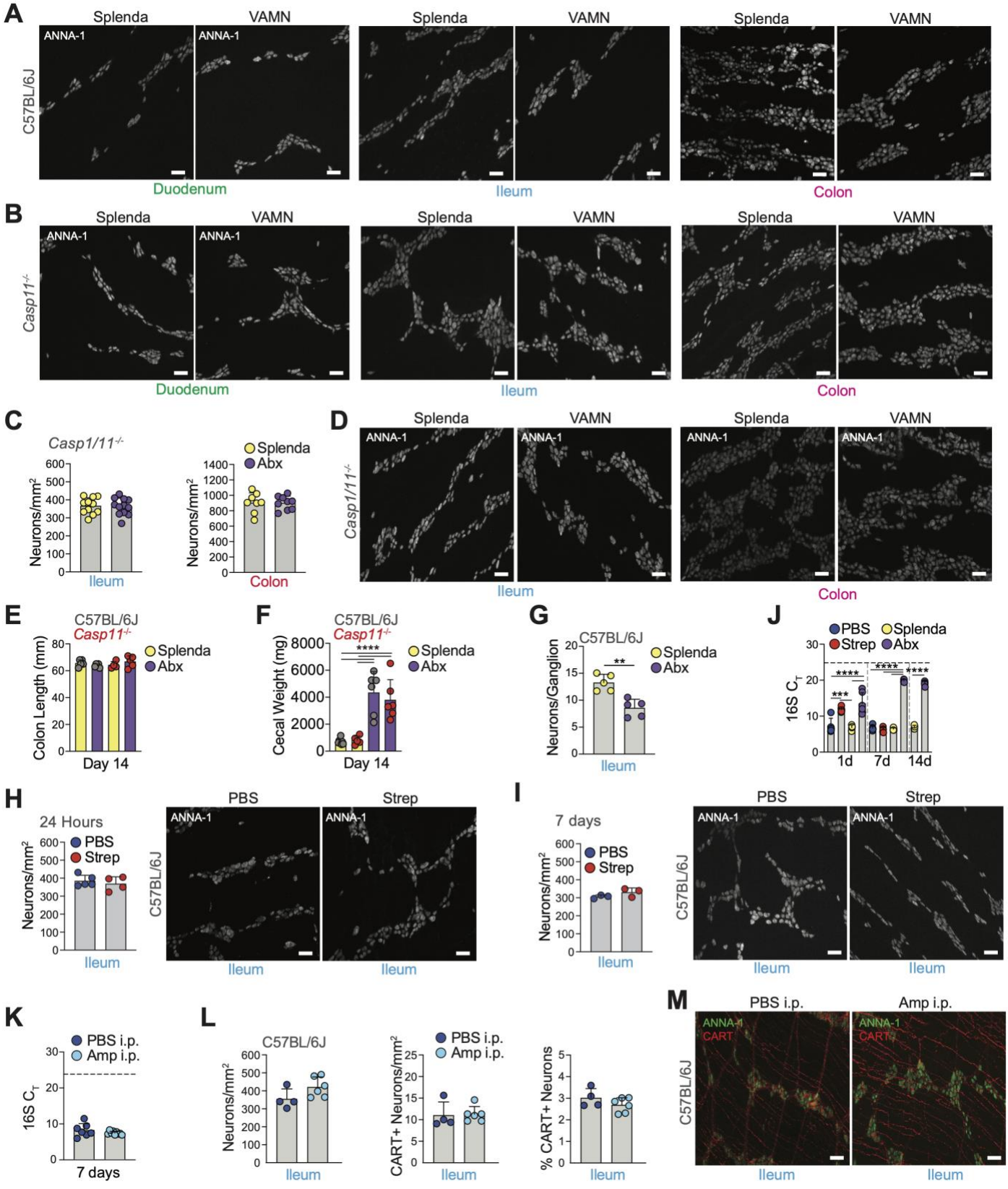

Fig. S5. Chronic oral administration of antibiotics leads to regionally restricted changes in iEAN. (A and B) Representative confocal IF images of myenteric iEAN (stained with anti-ANNA-1) in the duodenum, ileum, and colon of (A) C57BL/6J and (B) *Casp11*$^{-/-}$ mice treated with antibiotics or Splenda for two weeks. Images representative of n=5 per condition. Scale bars = 50 μm. (C) Number of myenteric iEAN per mm^2 in the ileum (left) and colon (right) of *Casp1/11*$^{-/-}$ mice treated with either Splenda or antibiotics for 2 weeks. (D)

Representative confocal IF images of myenteric iEAN in the ileum and colon of *Casp1/11*$^{-/-}$ mice. Images representative of n=5 per condition. Scale bars = 50 μm. (E and F) Measurements of (E) colonic length and (F) cecal weight of C57BL/6J and *Casp11*$^{-/-}$ mice treated with either Splenda or broad-spectrum antibiotics (vancomycin, ampicillin, metronidazole and neomycin) in the drinking water for 2 weeks. **** $P < 0.0001$ as calculated by two-way ANOVA with Tukey's multiple comparisons test. (G) Number of iEAN per ganglion of the ileum myenteric plexus of C57BL/6J SPF mice receiving either antibiotics or Splenda in the drinking water for 2 weeks. ** $P < 0.01$ as calculated by two-tailed unpaired t-test. (H and I) (Left) Number and (right) representative confocal immunofluorescence (IF) images of myenteric iEAN (stained with anti-ANNA-1) in the ileum of C57BL/6J SPF mice following a single oral dose of streptomycin and analyzed (H) 24 hours and (I) 7 days post gavage. Images representative of n = 3 per condition. Scale bars = 50 μm. (J) Cycle threshold (C_T) values of 16S quantitative real-time PCR (qPCR) from fecal samples of C57BL/6J SPF mice treated with a single oral gavage of streptomycin/PBS or broad-spectrum antibiotics (VAMN)/Splenda in the drinking water and analyzed at the indicated time points. Dotted line, average C_T value of pooled germ-free control samples. *** $P < 0.001$, **** $P < 0.0001$ as calculated by one-way ANOVA with Tukey's multiple comparisons test. (K to M) C57BL/6J SPF mice were treated with 1 g/kg ampicillin/PBS or PBS by i.p. injection for 7 consecutive days. (K) C_T values of 16S qPCR from fecal samples. Dotted line indicates average C_T value of pooled GF control samples; (L) Number of (left) myenteric iEAN in the ileum, (middle) CART+ iEAN per mm^2 and (right) CART+ iEAN as a percentage of total iEAN. (M) Representative confocal IF images of tissue analyzed in (L). Scale bars = 50 μm. Images representative of n= 4 per condition.

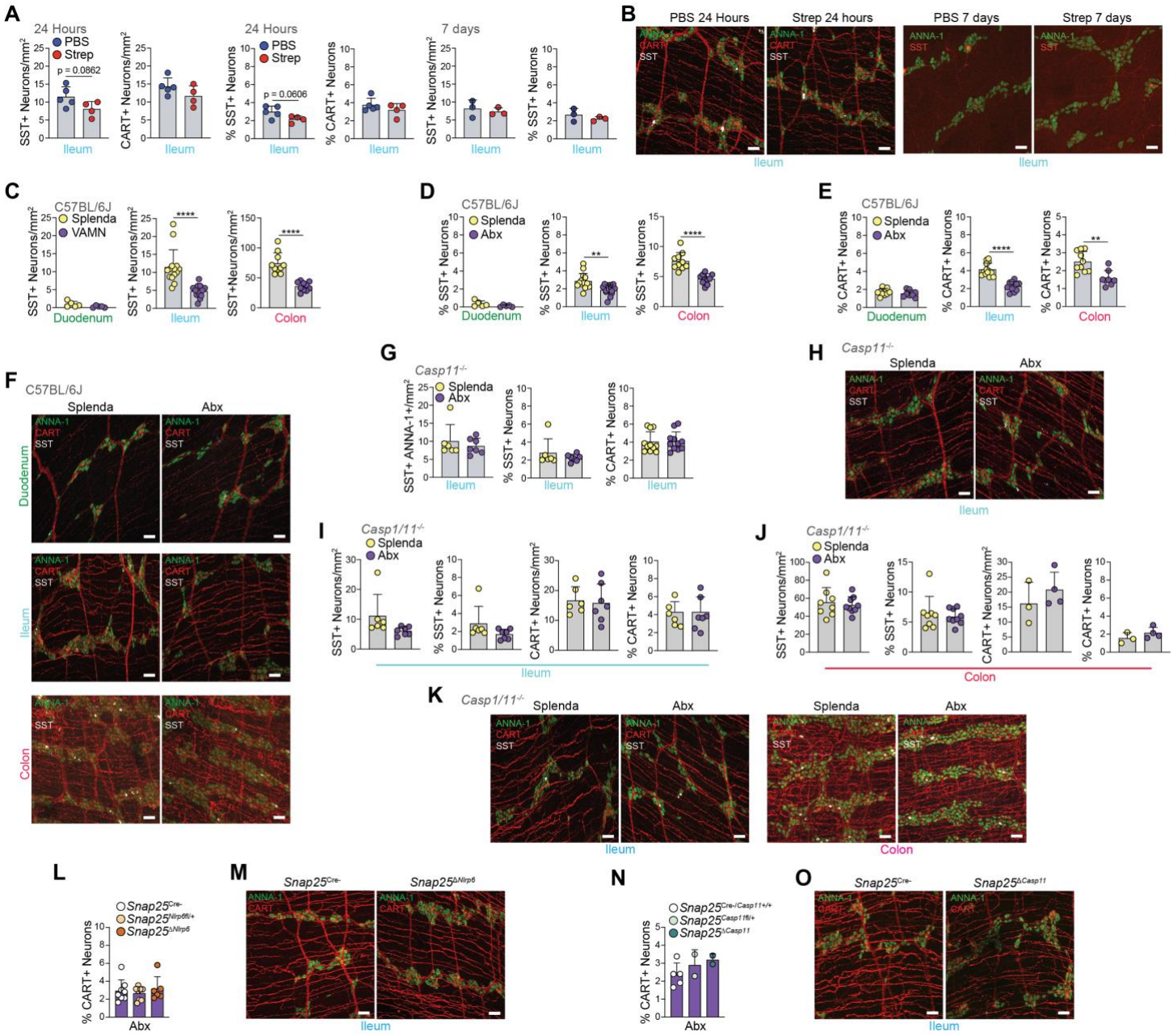

Fig. S6. Microbial depletion results in a NLRP6-Casp11-dependent loss of iEAN subsets. (A) Number and percentage of SST+ and CART+ iEAN of the ileum myenteric plexus of C57BL/6J SPF mice treated with a single oral gavage of PBS or streptomycin and analyzed 24 hours or 7 days post gavage (SST+ number and percentage only, right 2 panels). (B) Representative confocal IF images of tissue analyzed in (A). Scale bars = 50 µm. (C to E) C57BL/6J SPF mice were treated with antibiotics or Splenda for two weeks. (C) Number and (D and E) percentage of (C and D) SST+ and (E) CART+ iEAN out of total iEAN in the duodenum, ileum and colon. ** $P < 0.01$, *** $P < 0.001$, **** $P < 0.0001$ as calculated by two-tailed unpaired t-test (C) or Mann-Whitney test (D and E). (F) Representative confocal IF images of tissue analyzed in (C to E). Scale bars = 50 µm. (G) Number (SST, left) and Percentage of (middle) SST+ and (right) CART+ iEAN in the ileum myenteric plexus of *Casp11*$^{-/-}$ mice treated with antibiotics or Splenda for two weeks. (H) Representative confocal IF images of tissue analyzed in (G). Scale bars = 50 µm. (I and J) Number and percentage of (left) SST+ and (right) CART+ iEAN in the (I) ileum and (J) colon of *Casp1/11*$^{-/-}$ mice treated with antibiotics or Splenda for two weeks. (K) Representative confocal IF images of tissue analyzed in (I and J). Scale bars = 50 µm. (L and N) Percentage of CART+ iEAN out of total iEAN of the ileum myenteric plexus of (L) *Snap25*$^{\text{Cre}-}$, *Snap25*$^{Nlrp6\,fl/+}$, and *Snap25*$^{\Delta Nlrp6}$ and (N) *Snap25*$^{\text{Cre}-}$, *Snap25*$^{Casp11fl/+}$, and *Snap25*$^{\Delta Casp11}$ mice after two weeks of antibiotic treatment. (M and O) Representative confocal IF images of tissue analyzed in (L and N). Scale bars = 50 µm.

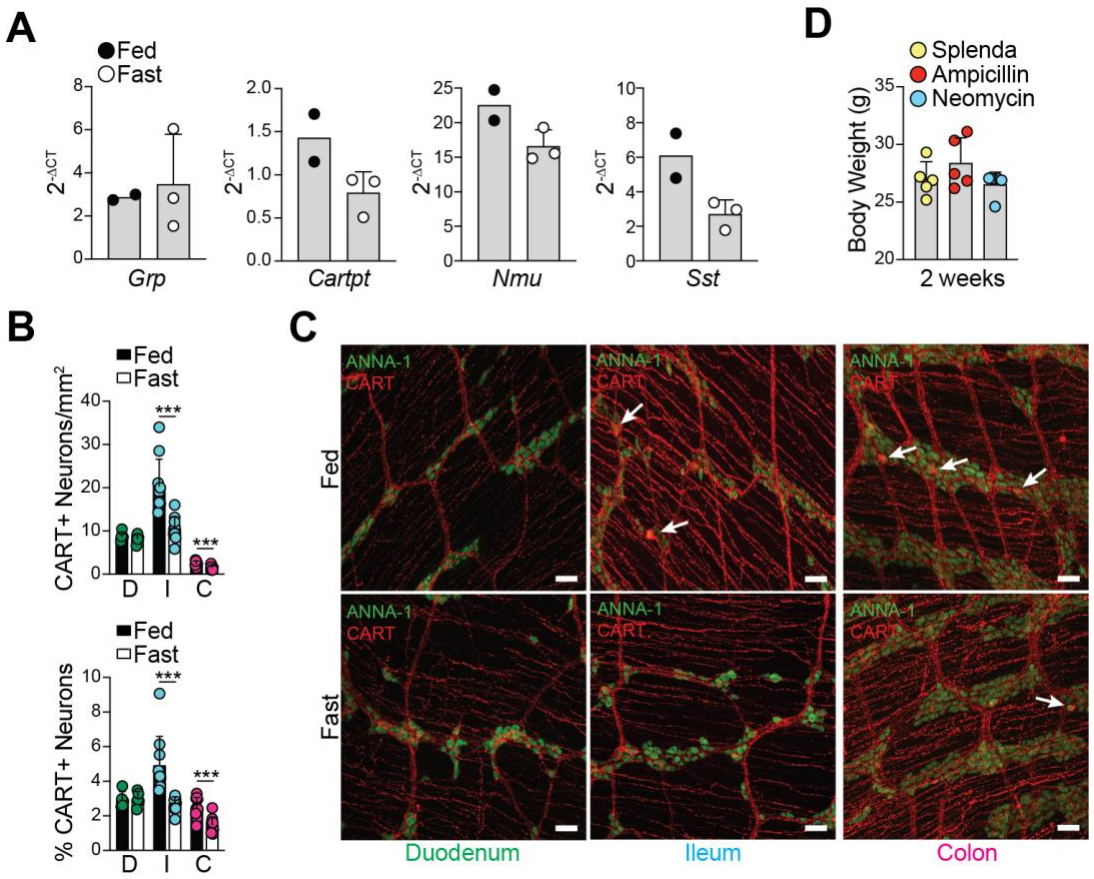

Fig. S7. Effects of fasting on distal intestine iEAN neuropeptide levels. (A) TRAP-qPCR analysis of the indicated neuropeptide genes of the ileum *muscularis externa* isolated from *Snap25*$^{RPL22\text{-}HA}$ mice with *ad libitum* food access or following overnight fasting. Data represented as log-transformed expression relative to *Rpl32*. (B) Number (top) and percentage (bottom) of CART+ myenteric iEAN in the duodenum (D), ileum (I), and colon (C) of C57BL/6J SPF mice with *ad libitum* food access or following overnight fasting. ** $P < 0.01$, *** $P < 0.001$, **** $P < 0.0001$ as calculated by unpaired t-test (number) or Mann-Whitney test (percentage). (C) Representative whole-mount IF images of the myenteric plexus quantified in (B). Scale bars = 50 μm. Images representative of at least n = 5/condition. (D) Body weights of C57BL/6J SPF mice treated with either ampicillin, neomycin, or Splenda in the drinking water for 2 weeks.

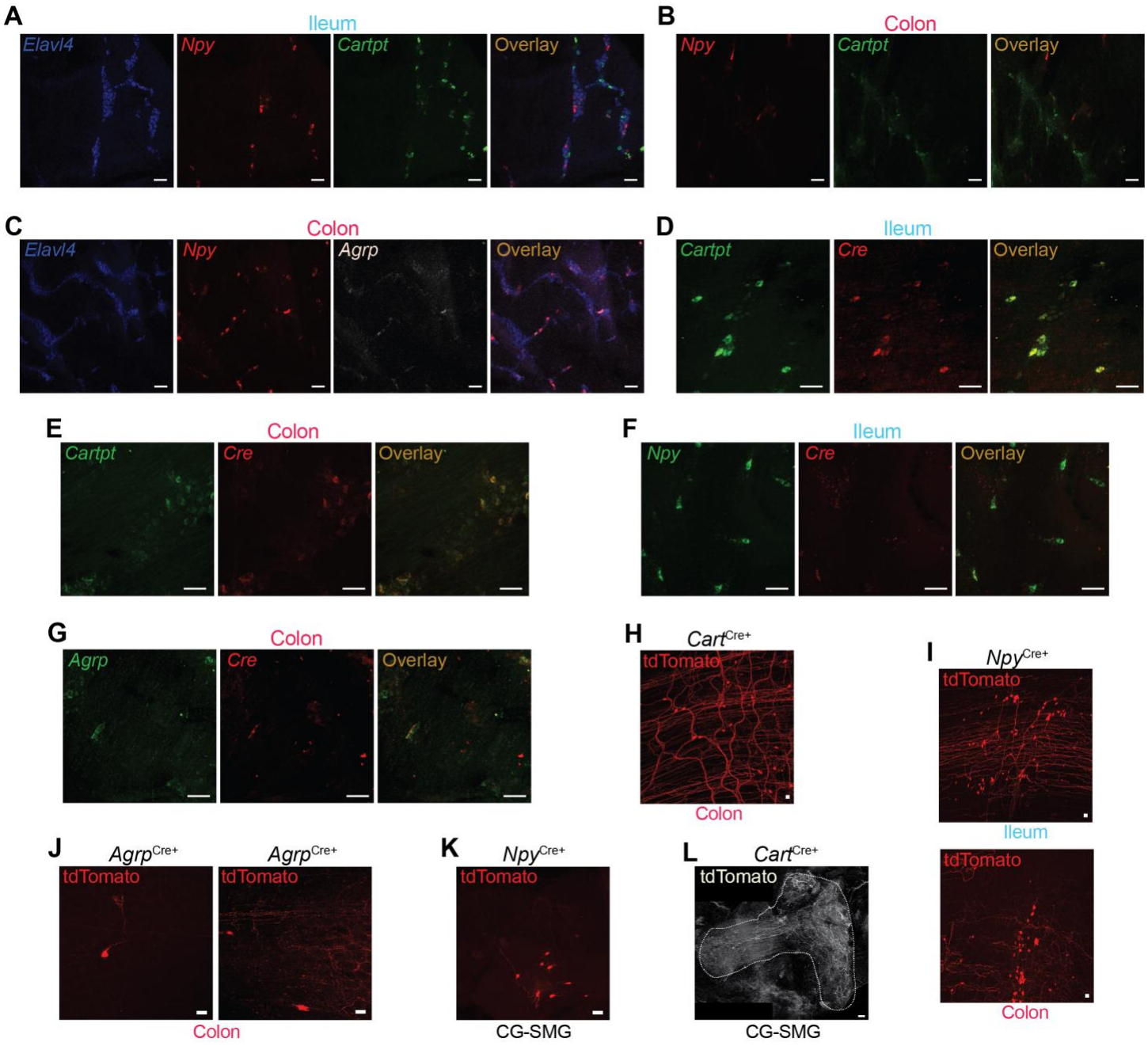

Fig. S8. Characterization of neuropeptide expression and patterning in the distal intestine. (A to C) RNAscope *in situ* hybridization whole-mount IF images of the indicated intestinal segments from C57BL/6J SPF mice using probes for (A and B) *Elavl4*, *Npy*, and *Cartpt* in the (A) ileum and (B) colon or *Elavl4*, *Npy*, and *Agrp* in the colon (C). Scale bars = 50 μm. (D to G) RNAscope *in situ* hybridization whole-mount IF images of intestinal segments from (D and E) *Cart*$^{Cre+}$, (F) *Npy*$^{Cre+}$, and (G) *Agrp*$^{Cre+}$ mice, from the (D and F) ileum and (E and G) colon using probes for *Cre* and (D and E) *Cartpt*, (F) *Npy* and (G) *Agrp*. Scale bars = 50 μm. (H and I) Immunofluorescence whole-mount images of the (H) colon from *Cart*$^{Cre+}$ mice, and (I) (top) ileum and (bottom) colon of *Npy*$^{Cre+}$ mice injected with AAVrg-FLEX-tdTomato into the duodenum, ileum, and colon. Scale bar = 50 μm. (J) Whole-mount IF images of the colon from *Agrp*$^{Cre+}$ mice injected with AAVrg-FLEX-tdTomato into the mid-colon. Scale bars = 50 μm. (K and L) Whole-mount IF image of the CG-SMG from (K) *Npy*$^{Cre+}$ and (L) *Cart*$^{Cre+}$ mice injected with AAVrg-FLEX-tdTomato into the duodenum, ileum, and colon. Scale bars = 50 (K) or 100 (L) μm.

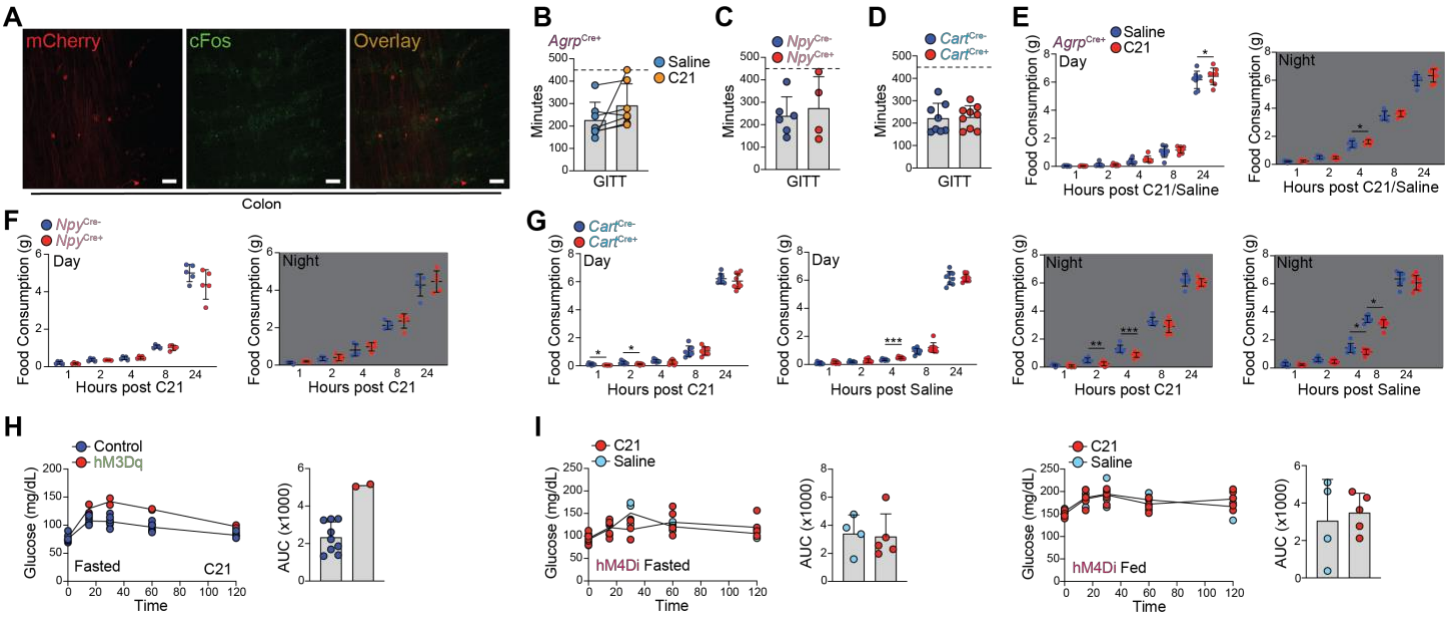

Fig. S9. Functional characterization of distal intestine iEAN. (A) Whole-mount immunofluorescence (IF) image 3 hours post administration of 1 mg^{-kg} compound 21 (C21) of cFos (green, stained with antibody) and mCherry (red, stained with antibody) in the colon myenteric plexus from *Agrp*$^{Cre+}$ mice injected with AAV9-hSyn-DIO-hM3Dq-mCherry into the mid-colon. Scale bars = 50 µm. (B to D) Gastrointestinal transit time (GITT) of (B) *Agrp*$^{Cre+}$, (C) *Npy*$^{Cre+}$, and (D) *Cart*$^{Cre+}$ mice injected with AAV9-hSyn-DIO-hM3Dq-mCherry into the ileum and colon. (E to G) Food consumption during (left) day or (right) night, post administration of 1 mg^{-kg} C21 or saline in (E) *Agrp*$^{Cre+}$, (F) *Npy*$^{Cre+}$, (G) *Cart*$^{Cre+}$ mice injected with AAV9-hSyn-DIO-hM3Dq-mCherry into the ileum and colon. * $P < 0.05$, ** $P < 0.01$, *** $P < 0.001$ as calculated by unpaired t-test. (H) (Left) Blood glucose levels and (right) AUC calculation of graph on the left of *Cart*$^{Cre+}$ mice overnight fasted injected with AAV9-hSyn-DIO-hM3Dq-mCherry into the ileum and colon, followed by administration of 1 mg^{-kg} C21, analyzed at the indicated timepoints. (I) Blood glucose levels and corresponding AUC calculation of *Cart*$^{Cre+}$ mice injected with AAV9-hSyn-DIO-hM4Di-mCherry into the ileum and (left) overnight fasted or (right) fed, followed by the administration of 1 mg^{-kg} C21, and analyzed at the indicated timepoints.

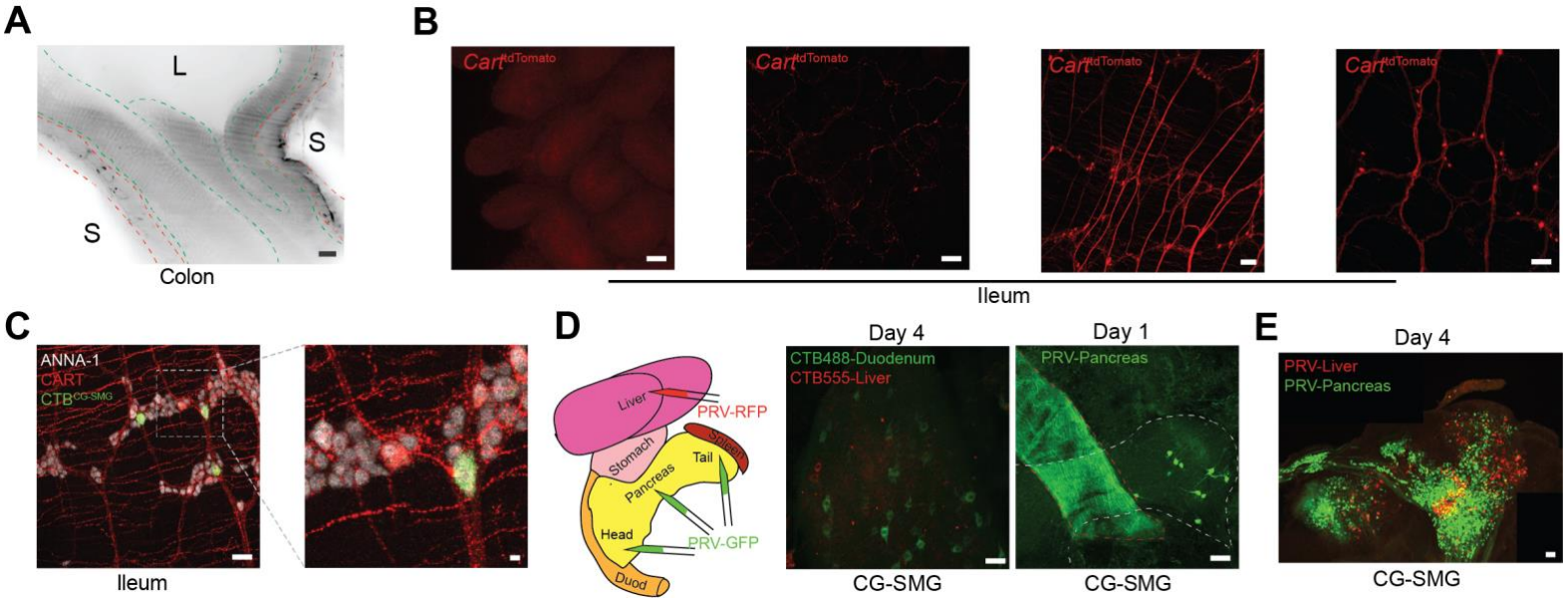

Fig. S10. Expression of CART is restricted to iEAN of the myenteric plexus. (A) Representative AdipoClear-cleared light-sheet image of the colon of *Cart*$^{Cre+}$ mice injected with AAV9-hSyn-DIO-hM3Dq-mCherry into the ileum and colon. Scale bar = 200 µm. L, intestinal lumen; S, serosa. Dotted red line outlines region containing the myenteric plexus. Dotted green line outlines region containing the mucosa and epithelium. (B) Representative whole-mount native fluorescence images of the intestinal (left) villi, (middle-left) submucosa and (middle- and far-right) ileum myenteric region of *Cart*^{tdTomato} mice. Scale bars = 50 µm. Images representative of at least n = 3 mice. (C) Representative whole-mount IF image of the ileum myenteric plexus highlighting CART+ fiber (red) in close proximity to a viscerofugal neuron (green) from C57BL/6J mice. Scale bar (left) = 50 µm. Scale bar (inset on the right) = 10 µm. (D) (left) Schematic of fluorescent PRV injection into the liver and pancreas. (middle) Representative whole-mount (native fluorescence) images of the CG-SMG 4 days post injection of CTB488/555 into the duodenum/liver and (right) one day post injection of PRV-GFP into the pancreas of C57BL/6J SPF mice. Scale bars = 50 µm. (E) Whole-mount IF image of the CG-SMG 4 days post injection of PRV-GFP into the pancreas and PRV-RFP into the liver. Scale bar = 100 µm.

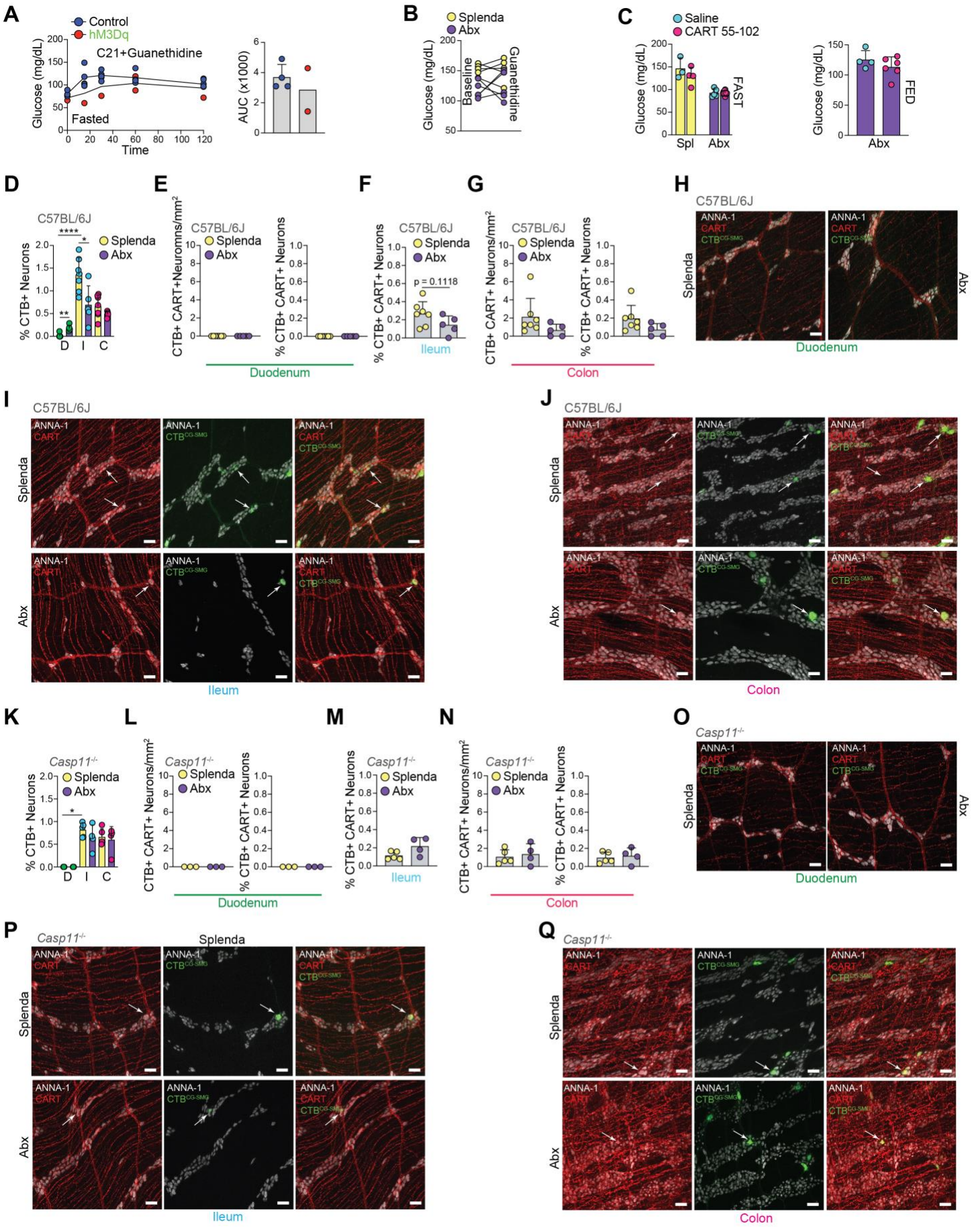
A
Control
hM3Dq
C21+Guanethidine
Fasted
Glucose (mg/dL)
Time
AUC (x1000)
B
Splenda
Abx
Baseline
Guanethidine
Glucose (mg/dL)
C
Saline
CART 55-102
FAST
FED
Spl
Abx
D
C57BL/6J
% CTB+ Neurons
D I C
E
CTB+ CART+Neuromns/mm2
% CTB+ CART+ Neurons
Duodenum
F
% CTB+ CART+ Neurons
p = 0.1118
Ileum
G
CTB+ CART+ Neurons/mm2
% CTB+ CART+ Neurons
Colon
H
C57BL/6J
ANNA-1
CART
CTBCG-SMG
Splenda
Abx
Duodenum
I
C57BL/6J
Ileum
J
C57BL/6J
Colon
K
Casp11-/-
L
M
N
O
P
Q

Fig. S11. Analysis of viscerofugal CART+ iEAN across intestinal regions. (A) (Left) Blood glucose levels and (right) corresponding area under the curve (AUC) calculation of *Cart*$^{Cre+}$ mice fasted overnight, followed by administration of guanethidine (30 mg^{-kg}) and C21 (1 mg^{-kg}), analyzed at the indicated timepoints. Mice were injected with AAV9-hSyn-DIO-hM3Dq-mCherry into the ileum and colon. (B) Fasted blood glucose levels of C57BL/6J SPF mice treated with antibiotics for 2 weeks and i.p. injected with guanethidine 1 hour prior to analysis. (C) Blood glucose levels 1 hour after i.p. injection of CART 55-102 peptide (25 μg/kg) in fasted (left) or fed (right) C57BL/6J SPF mice treated with broad-spectrum antibiotics or Splenda. (D) Percentage of CTB-AF647+ positive neurons in the duodenum (D), ileum (I), and colon (C) of C57BL/6J SPF mice treated with antibiotics or Splenda for 2 weeks. * $P < 0.05$, ** $P < 0.01$, **** $P < 0.0001$ as calculated by Mann-Whitney test (Abx vs Splenda within intestine region comparisons) or Kruskal-Wallis with Dunn's multiple comparisons test (Splenda region CTB comparisons). (E to G) Number and percentage CTB-AF647+ CART+ double-positive neurons in the (E) duodenum, (F) ileum (number only) and (G) colon after injection of CTB into the CG-SMG of C57BL/6J SPF mice treated with antibiotics (VAMN) or Splenda for two weeks. (H to J) Representative whole-mount IF images of the myenteric plexus quantified in (E to G). White arrows indicate CTB+ CART+ neurons. Scale bars = 50 μm. Images representative of at least n = 5/condition. (K) Percentage of CTB-AF647+ positive neurons in the duodenum (D), ileum (I), and colon (C) of *Casp11*$^{-/-}$ mice treated with antibiotics or Splenda for 2 weeks. * $P < 0.05$ as calculated by Kruskal-Wallis with Dunn's multiple comparisons test. (L to N) Number and percentage of CTB-AF647+ CART+ double-positive neurons in the (L) duodenum, (M) ileum (number only) and (N) colon after injection of CTB into the CG-SMG of *Casp11*$^{-/-}$ mice treated with antibiotics (VAMN) or Splenda for two weeks. (O to Q) Representative whole-mount IF images of the myenteric plexus quantified in (K to N). White arrows indicate CTB+ CART+ neurons. Scale bars = 50 μm. Images representative of at least n = 5 per condition.

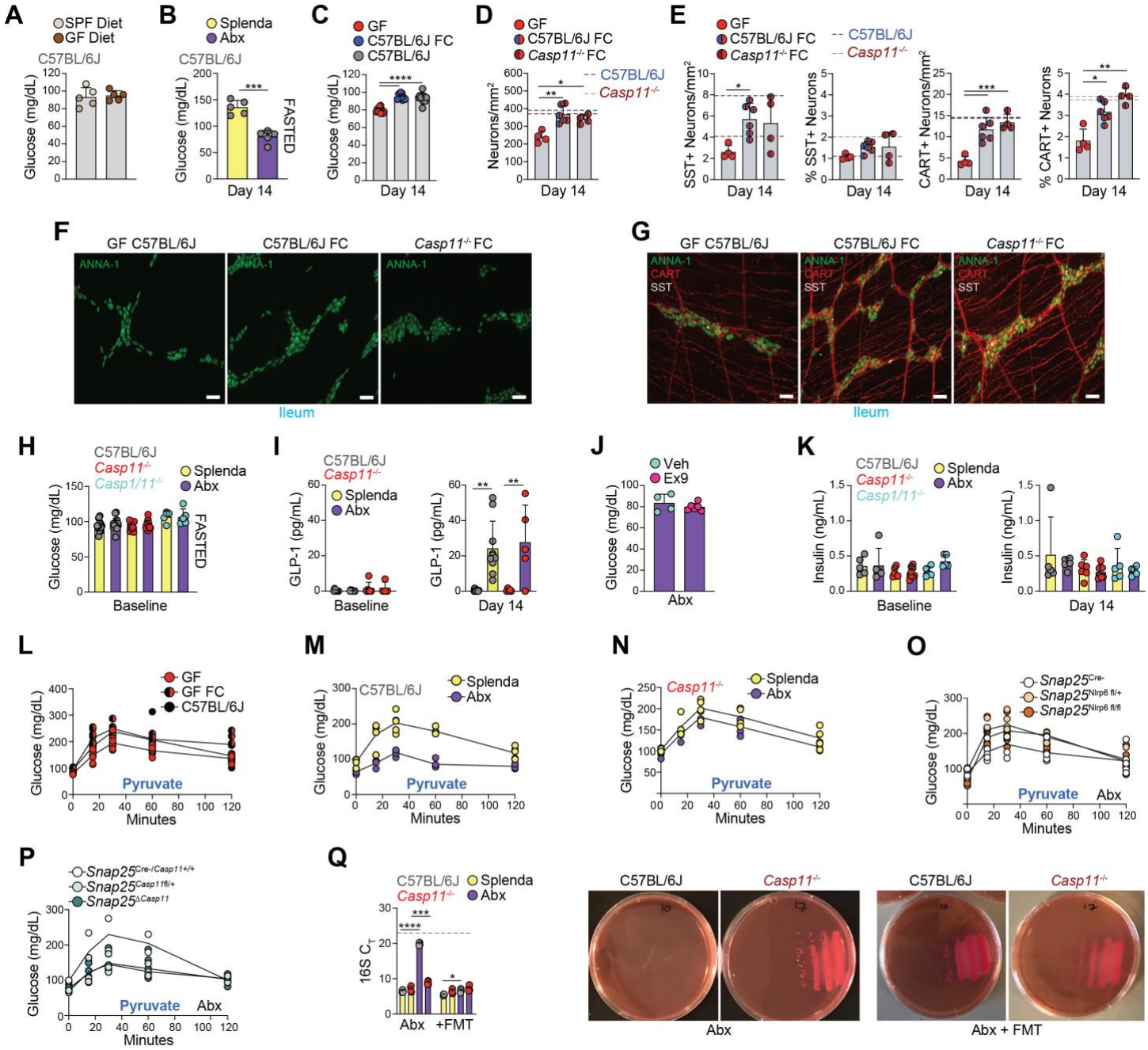

Fig. S12. Microbiota-dependent maintenance of iEAN and glucose metabolism is dependent on NLRP6 and Casp11. (A) Blood glucose levels of overnight fasted C57BL/6J SPF mice receiving regular chow diet or 4 days after switching to autoclaved germ-free diet. (B) Blood glucose levels of fasted C57BL/6J SPF mice treated with broad-spectrum antibiotics or Splenda for 2 weeks. *** $P < 0.001$ as calculated by two-tailed unpaired t-test. (C) Blood glucose levels of overnight-fasted C57BL/6J GF, GF colonized (C57BL/6J microbiota, fecal colonization, FC), and C57BL/6J housed in ISOcages, 2 weeks post colonization. **** $P < 0.0001$ as calculated one-way ANOVA with Tukey's multiple comparisons test. (D to G) C57BL/6J GF mice were colonized with microbiota from C57BL/6J or *Casp11*$^{-/-}$ (fecal colonization, FC) mice. Dotted blue lines, C57BL/6J (FC donor) baselines. Dotted red lines, *Casp11*$^{-/-}$ (FC donor) baselines. (D) Number of myenteric plexus iEAN per mm^2; (E) Number and percentage of (left) SST+ and (right) CART+ myenteric plexus iEAN per mm^2 and as a percentage of total iEAN. * $P < 0.05$, ** $P < 0.01$, *** $P < 0.001$ as calculated by one-way ANOVA with Tukey's multiple comparisons test (number) or Kruskal-Wallis with Dunn's multiple comparisons test (percentage). (F and G) Representative whole-mount IF images of the myenteric plexus quantified in (D to E). Scale bars = 50 µm. Images representative of at least n = 4/condition. (H) Blood glucose

levels of overnight fasted C57BL/6J, *Casp1/11*$^{-/-}$, and *Casp11*$^{-/-}$ mice treated with Splenda in the drinking water before switching experimental groups on antibiotics (VAMN) in the drinking water. (I) Plasma levels of GLP-1 in C57BL/6J and *Casp11*$^{-/-}$ mice at baseline and after treatment with antibiotics or Splenda for 2 weeks. ** $P < 0.01$ as calculated by one-way ANOVA with Tukey's multiple comparisons test. (J) Blood glucose levels of C57BL/6J mice previously treated with broad-spectrum antibiotics for 2 weeks, 1-hour post Exendin-9-39 treatment. (K) Plasma levels of insulin in C57BL/6J, *Casp1/11*$^{-/-}$, and *Casp11*$^{-/-}$ mice at baseline and after treatment with antibiotics or Splenda for 2 weeks. (L to P) Blood glucose levels following overnight fasting at baseline and at the indicated timepoints post i.p. administration of 1 g/kg pyruvate/PBS in (L) GF, GF post colonization with C57BL/6J microbiota (GF FC), or C57BL/J6 mice, (M) C57BL/6J mice treated with antibiotics or Splenda for 2 weeks, (N) *Casp11*$^{-/-}$ mice treated with antibiotics or Splenda for 2 weeks, (O) *Snap25*$^{\text{Cre}-}$, *Snap25*$^{Nlrp6fl/+}$ or *Snap25*$^{\Delta Nlrp6}$ mice treated with antibiotics for 2 weeks, and (P) *Snap25*$^{\text{Cre}-}$, *Snap25*$^{Casp11fl/+}$ or *Snap25*$^{\Delta Casp11}$ mice treated with antibiotics for 2 weeks. (Q) (Left) C_T values of 16S qPCR from fecal samples of C57BL/6J and *Casp11*$^{-/-}$ mice treated with antibiotics or Splenda for 4 weeks, and after fecal transfer between *Casp11*$^{-/-}$ and C57BL/6J mice to normalize the microbiota. Dotted line indicates average C_T value of pooled germ-free control samples; * $P < 0.05$, *** $P < 0.001$, **** $P < 0.0001$ as calculated by two-way ANOVA with Tukey's test for multiple comparisons; (Right) representative agar plates confirming colonization with antibiotic-resistant bacterial species.

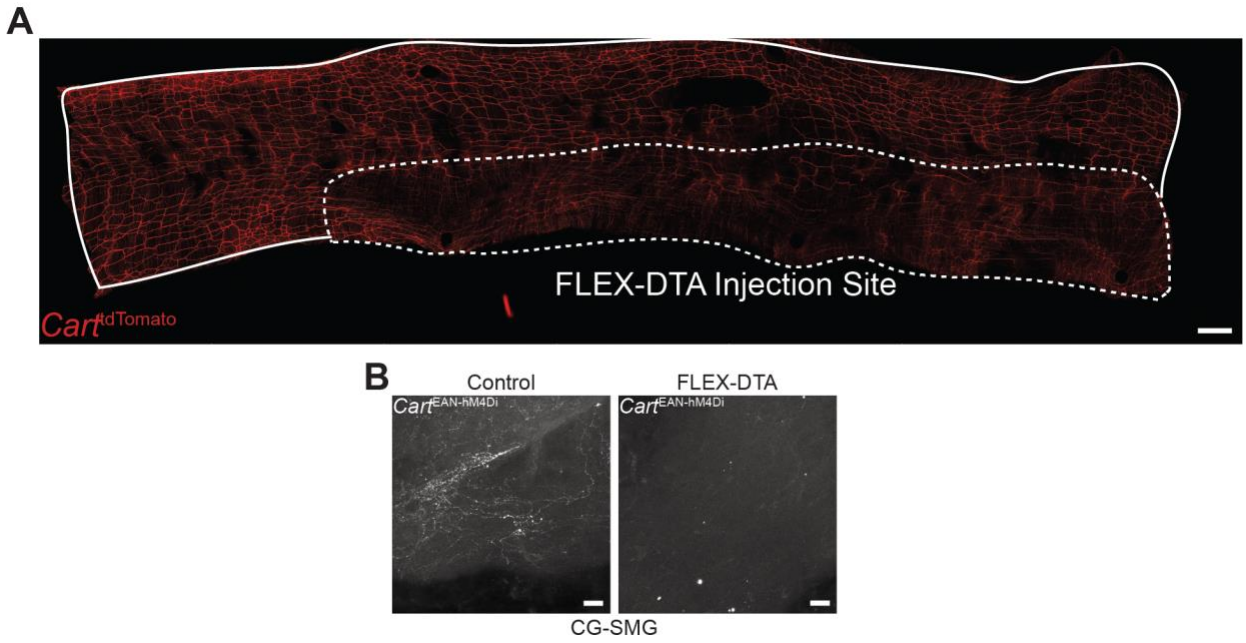

Fig. S13. Viral ablation of CART+ iEAN. (A) Representative whole-mount confocal immunofluorescence (IF) image of the ileum of *Cart*^{tdTomato} mice injected with AAV5-FLEX-DTA virus into the ileum. Scale bar = 1 mm. Continuous white line outlines whole tissue, dotted white indicates virus injection site. (B) Representative whole-mount confocal IF images of the CG-SMG of *Cart*$^{Cre+}$ mice injected with AAV9-DIO-hSyn-hM4Di-mCherry in the ileum and colon (*Cart*$^{EAN\text{-}hM4Di}$) following a subsequent injection with control virus or AAV5-FLEX-DTA into the ileum and colon two weeks later. Scale bars = 50 μm.

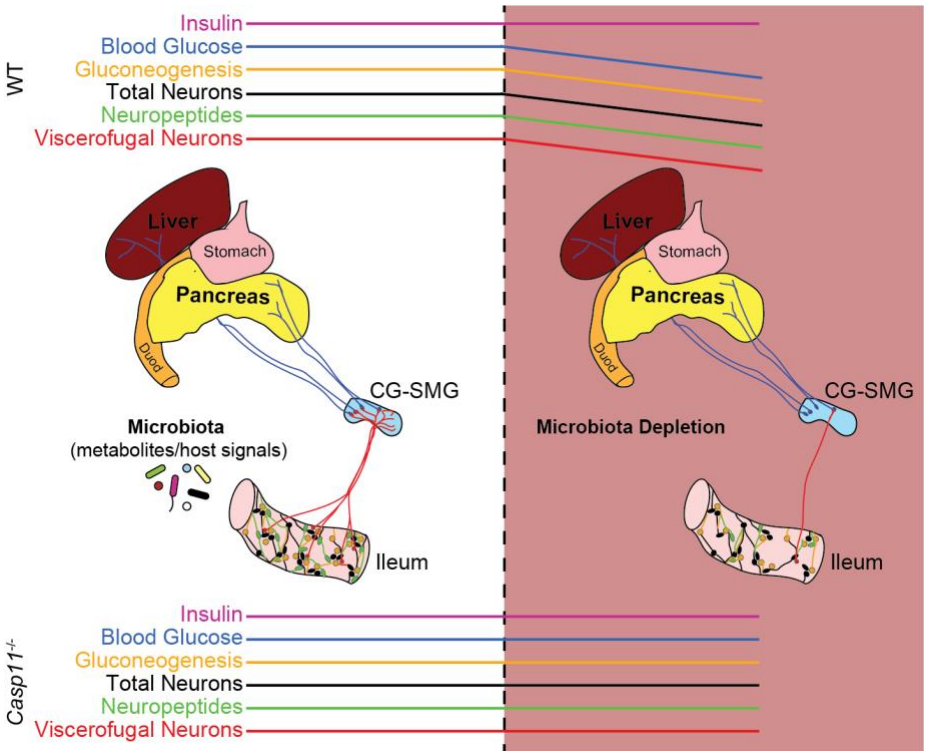

Fig. S14. Study schematic. In the absence of a microbiota there is a reduction in gluconeogenesis, which is coupled to a loss of subset specific, viscerofugal and total EAN. CART+ viscerofugal neurons are anatomically connected to the liver (gluconeogenesis regulation) and pancreas (insulin regulation) and are therefore poised to modulate blood glucose. The loss of gut viscerofugal input to the CG-SMG results in a decreased capacity for sympathetic-mediated gluconeogenesis via a CG-SMG-liver circuit. Rescuing iEAN loss through global or neuronal-specific deletion of Casp11 prevents changes in glucose levels found upon microbial depletion.

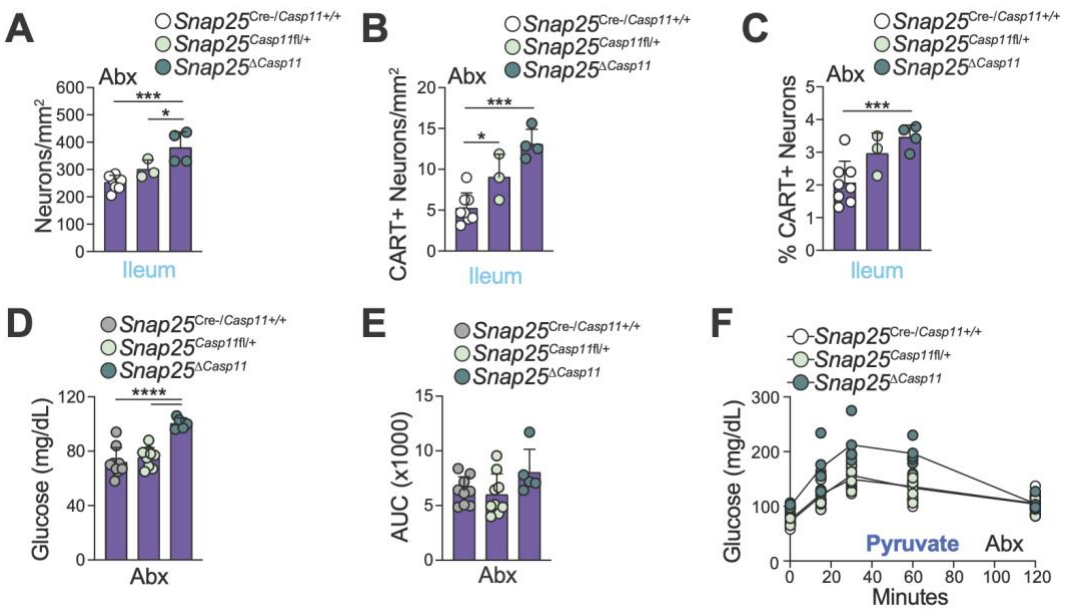

Fig. S15. Increased *n* for *Snap25*$^{\Delta Casp11}$ experiments. (A-C) Increased *n* for original submission panels (A: Fig. 3C, B: Fig. 3H, C: fig. S6N). Ileal myenteric (A) total iEAN numbers, (B) CART+ iEAN numbers, and (C) percentage of CART+ iEAN out of total iEAN in *Snap25*$^{Cre-}$, *Snap25*$^{Casp11fl/+}$, and *Snap25*$^{\Delta Casp11}$ mice after two weeks of antibiotic treatment. (D-F) Increased *n* for original submission panels (D: Fig. 6F, D: Fig. 6K, F: fig. S12P). (D) Blood glucose (BG) levels at baseline, (E) IP-PTT AUC analysis, and (F) IP-PTT BG curves of overnight fasted *Snap25*$^{Cre-}$, *Snap25*$^{Casp11fl/+}$ and *Snap25*$^{\Delta Casp11}$ mice treated with antibiotics for 2 weeks. * $P < 0.05$, ** $P < 0.01$, **** $P < 0.0001$ as calculated by one-way ANOVA with Tukey's multiple comparisons test (A,B,D) or Kruskal-Wallis with Dunn's multiple comparisons test (C).

external_gene_name	ensembl_gene_id	description
Wif1	ENSMUSG00000020218	Wnt inhibitory factor 1 [Source:MGI Symbol;Acc:MGI:1344332]
Krt19	ENSMUSG00000020911	keratin 19 [Source:MGI Symbol;Acc:MGI:96693]
Otof	ENSMUSG00000062372	otoferlin [Source:MGI Symbol;Acc:MGI:1891247]
Ucn3	ENSMUSG00000044988	urocortin 3 [Source:MGI Symbol;Acc:MGI:1932970]
Pnoc	ENSMUSG00000045731	prepronociceptin [Source:MGI Symbol;Acc:MGI:105308]
Esr1	ENSMUSG00000019768	estrogen receptor 1 (alpha) [Source:MGI Symbol;Acc:MGI:1352467]
Ndufa4l2	ENSMUSG00000040280	NADH dehydrogenase (ubiquinone) 1 alpha subcomplex, 4-like 2 [Source:MGI Symbol;Acc:MGI:3039567]
Uts2b	ENSMUSG00000056423	urotensin 2B [Source:MGI Symbol;Acc:MGI:2677064]
Dlx5	ENSMUSG00000029755	distal-less homeobox 5 [Source:MGI Symbol;Acc:MGI:101926]
Grin2c	ENSMUSG00000020734	glutamate receptor, ionotropic, NMDA2C (epsilon 3) [Source:MGI Symbol;Acc:MGI:95822]
Gabra3	ENSMUSG00000031343	gamma-aminobutyric acid (GABA) A receptor, subunit alpha 3 [Source:MGI Symbol;Acc:MGI:95615]
Ecel1	ENSMUSG00000026247	endothelin converting enzyme-like 1 [Source:MGI Symbol;Acc:MGI:1343461]
Pmaip1	ENSMUSG00000024521	phorbol-12-myristate-13-acetate-induced protein 1 [Source:MGI Symbol;Acc:MGI:1930146]
Necab1	ENSMUSG00000040536	N-terminal EF-hand calcium binding protein 1 [Source:MGI Symbol;Acc:MGI:1916602]
Cckar	ENSMUSG00000029193	cholecystokinin A receptor [Source:MGI Symbol;Acc:MGI:99478]
Rasgrp3	ENSMUSG00000071042	RAS, guanyl releasing protein 3 [Source:MGI Symbol;Acc:MGI:3028579]
Rnf128	ENSMUSG00000031438	ring finger protein 128 [Source:MGI Symbol;Acc:MGI:1914139]
Eya1	ENSMUSG00000025932	EYA transcriptional coactivator and phosphatase 1 [Source:MGI Symbol;Acc:MGI:109344]
Gbx1	ENSMUSG00000067724	gastrulation brain homeobox 1 [Source:MGI Symbol;Acc:MGI:95667]
Pgf	ENSMUSG00000004791	placental growth factor [Source:MGI Symbol;Acc:MGI:105095]
Rxfp1	ENSMUSG00000034009	relaxin/insulin-like family peptide receptor 1 [Source:MGI Symbol;Acc:MGI:2682211]
Trpv1	ENSMUSG00000005952	transient receptor potential cation channel, subfamily V, member 1 [Source:MGI Symbol;Acc:MGI:1341787]
Fam19a4	ENSMUSG00000046500	family with sequence similarity 19, member A4 [Source:MGI Symbol;Acc:MGI:2444563]
Adamts14	ENSMUSG00000059901	a disintegrin-like and metallopeptidase (reprolysin type) with thrombospondin type 1 motif, 14 [Source:MGI Symbol;Acc:MGI:2179942]
Kcnj14	ENSMUSG00000058743	potassium inwardly-rectifying channel, subfamily J, member 14 [Source:MGI Symbol;Acc:MGI:2384820]
Foxs1	ENSMUSG00000074676	forkhead box S1 [Source:MGI Symbol;Acc:MGI:95546]
Npy	ENSMUSG00000029819	neuropeptide Y [Source:MGI Symbol;Acc:MGI:97374]
Ptgdr	ENSMUSG00000071489	prostaglandin D receptor [Source:MGI Symbol;Acc:MGI:102966]
Sp5	ENSMUSG00000075304	trans-acting transcription factor 5 [Source:MGI Symbol;Acc:MGI:1927715]
Ntrk1	ENSMUSG00000028072	neurotrophic tyrosine kinase, receptor, type 1 [Source:MGI Symbol;Acc:MGI:97383]
Adra1b	ENSMUSG00000050541	adrenergic receptor, alpha 1b [Source:MGI Symbol;Acc:MGI:104774]
Gabbr2	ENSMUSG00000039809	gamma-aminobutyric acid (GABA) B receptor, 2 [Source:MGI Symbol;Acc:MGI:2386030]
Gprin3	ENSMUSG00000045441	GPRIN family member 3 [Source:MGI Symbol;Acc:MGI:1924785]
Nkain3	ENSMUSG00000055761	Na+/K+ transporting ATPase interacting 3 [Source:MGI Symbol;Acc:MGI:2444830]
Fam20a	ENSMUSG00000020614	family with sequence similarity 20, member A [Source:MGI Symbol;Acc:MGI:2388266]
Aard	ENSMUSG00000068522	alanine and arginine rich domain containing protein [Source:MGI Symbol;Acc:MGI:2181621]
Tmem132b	ENSMUSG00000070498	transmembrane protein 132B [Source:MGI Symbol;Acc:MGI:3609245]
Nt5dc2	ENSMUSG00000071547	5'-nucleotidase domain containing 2 [Source:MGI Symbol;Acc:MGI:1917271]
Hcn4	ENSMUSG00000032338	hyperpolarization-activated, cyclic nucleotide-gated K+ 4 [Source:MGI Symbol;Acc:MGI:1298209]
Gja3	ENSMUSG00000048582	gap junction protein, alpha 3 [Source:MGI Symbol;Acc:MGI:95714]
Ghsr	ENSMUSG00000051136	growth hormone secretagogue receptor [Source:MGI Symbol;Acc:MGI:2441906]
Npas1	ENSMUSG00000001988	neuronal PAS domain protein 1 [Source:MGI Symbol;Acc:MGI:109205]
Tacr3	ENSMUSG00000028172	tachykinin receptor 3 [Source:MGI Symbol;Acc:MGI:892968]
Bmper	ENSMUSG00000031963	BMP-binding endothelial regulator [Source:MGI Symbol;Acc:MGI:1920480]
Kcnj16	ENSMUSG00000051497	potassium inwardly-rectifying channel, subfamily J, member 16 [Source:MGI Symbol;Acc:MGI:1314842]
Crhbp	ENSMUSG00000021680	corticotropin releasing hormone binding protein [Source:MGI Symbol;Acc:MGI:88497]
Gpr6	ENSMUSG00000046922	G protein-coupled receptor 6 [Source:MGI Symbol;Acc:MGI:2155249]
Dclk3	ENSMUSG00000032500	doublecortin-like kinase 3 [Source:MGI Symbol;Acc:MGI:3039580]
Arg2	ENSMUSG00000021125	arginase type II [Source:MGI Symbol;Acc:MGI:1330806]
Slc4a11	ENSMUSG00000074796	solute carrier family 4, sodium bicarbonate transporter-like, member 11 [Source:MGI Symbol;Acc:MGI:2138987]
Asb4	ENSMUSG00000042607	ankyrin repeat and SOCS box-containing 4 [Source:MGI Symbol;Acc:MGI:1929751]
A930017K11Rik	ENSMUSG00000025727	RIKEN cDNA A930017K11 gene [Source:MGI Symbol;Acc:MGI:2442713]
Maob	ENSMUSG00000040147	monoamine oxidase B [Source:MGI Symbol;Acc:MGI:96916]
Maoa	ENSMUSG00000025037	monoamine oxidase A [Source:MGI Symbol;Acc:MGI:96915]
Emilin2	ENSMUSG00000024053	elastin microfibril interfacer 2 [Source:MGI Symbol;Acc:MGI:2389136]
Lmo2	ENSMUSG00000032698	LIM domain only 2 [Source:MGI Symbol;Acc:MGI:102811]
Atm	ENSMUSG00000034218	ataxia telangiectasia mutated [Source:MGI Symbol;Acc:MGI:107202]
Pik3c2g	ENSMUSG00000030228	phosphatidylinositol-4-phosphate 3-kinase catalytic subunit type 2 gamma [Source:MGI Symbol;Acc:MGI:1203730]
Bcat1	ENSMUSG00000030268	branched chain aminotransferase 1, cytosolic [Source:MGI Symbol;Acc:MGI:104861]
Myh1	ENSMUSG00000056328	myosin, heavy polypeptide 1, skeletal muscle, adult [Source:MGI Symbol;Acc:MGI:1339711]
Brinp1	ENSMUSG00000028351	bone morphogenic protein/retinoic acid inducible neural specific 1 [Source:MGI Symbol;Acc:MGI:1928478]
Cnih3	ENSMUSG00000026514	cornichon family AMPA receptor auxiliary protein 3 [Source:MGI Symbol;Acc:MGI:1920228]
Slc35f4	ENSMUSG00000021852	solute carrier family 35, member F4 [Source:MGI Symbol;Acc:MGI:1922538]
Pde2a	ENSMUSG00000110195	phosphodiesterase 2A, cGMP-stimulated [Source:MGI Symbol;Acc:MGI:2446107]
C1ql2	ENSMUSG00000036907	complement component 1, q subcomponent-like 2 [Source:MGI Symbol;Acc:MGI:3032521]
Mrap2	ENSMUSG00000042761	melanocortin 2 receptor accessory protein 2 [Source:MGI Symbol;Acc:MGI:3609239]
Vmn2r29	ENSMUSG00000095730	vomeronasal 2, receptor 29 [Source:MGI Symbol;Acc:MGI:1923479]
Serpinf1	ENSMUSG00000000753	serine (or cysteine) peptidase inhibitor, clade F, member 1 [Source:MGI Symbol;Acc:MGI:108080]
Pkp1	ENSMUSG00000026413	plakophilin 1 [Source:MGI Symbol;Acc:MGI:1328359]
Slc35f3	ENSMUSG00000057060	solute carrier family 35, member F3 [Source:MGI Symbol;Acc:MGI:2444426]
Gck	ENSMUSG00000041798	glucokinase [Source:MGI Symbol;Acc:MGI:1270854]
Rasgrf1	ENSMUSG00000032356	RAS protein-specific guanine nucleotide-releasing factor 1 [Source:MGI Symbol;Acc:MGI:99694]
Mmd2	ENSMUSG00000039533	monocyte to macrophage differentiation-associated 2 [Source:MGI Symbol;Acc:MGI:1922354]
Capn6	ENSMUSG00000067276	calpain 6 [Source:MGI Symbol;Acc:MGI:1100850]
Sulf2	ENSMUSG00000006800	sulfatase 2 [Source:MGI Symbol;Acc:MGI:1919293]
Gpr149	ENSMUSG00000043441	G protein-coupled receptor 149 [Source:MGI Symbol;Acc:MGI:2443628]
Ackr3	ENSMUSG00000044337	atypical chemokine receptor 3 [Source:MGI Symbol;Acc:MGI:109562]
Atoh8	ENSMUSG00000037621	atonal bHLH transcription factor 8 [Source:MGI Symbol;Acc:MGI:1918343]
Moxd1	ENSMUSG00000020000	monooxygenase, DBH-like 1 [Source:MGI Symbol;Acc:MGI:1921582]
Dlx2	ENSMUSG00000023391	distal-less homeobox 2 [Source:MGI Symbol;Acc:MGI:94902]
Dync1i1	ENSMUSG00000029757	dynein cytoplasmic 1 intermediate chain 1 [Source:MGI Symbol;Acc:MGI:107743]
Inhbb	ENSMUSG00000037035	inhibin beta-B [Source:MGI Symbol;Acc:MGI:96571]
Gpr68	ENSMUSG00000047415	G protein-coupled receptor 68 [Source:MGI Symbol;Acc:MGI:2441763]
4930550C14Rik	ENSMUSG00000005131	RIKEN cDNA 4930550C14 gene [Source:MGI Symbol;Acc:MGI:1922561]
Stac	ENSMUSG00000032502	src homology three (SH3) and cysteine rich domain [Source:MGI Symbol;Acc:MGI:1201400]
Slc6a4	ENSMUSG00000020838	solute carrier family 6 (neurotransmitter transporter, serotonin), member 4 [Source:MGI Symbol;Acc:MGI:96285]
Spon1	ENSMUSG00000038156	spondin 1, (f-spondin) extracellular matrix protein [Source:MGI Symbol;Acc:MGI:2385287]
Bcas1	ENSMUSG00000013523	breast carcinoma amplified sequence 1 [Source:MGI Symbol;Acc:MGI:1924210]
Vsir	ENSMUSG00000020101	V-set immunoregulatory receptor [Source:MGI Symbol;Acc:MGI:1921298]
Plscr4	ENSMUSG00000032377	phospholipid scramblase 4 [Source:MGI Symbol;Acc:MGI:2143267]
Fst	ENSMUSG00000021765	follistatin [Source:MGI Symbol;Acc:MGI:95586]
Tnr	ENSMUSG00000015829	tenascin R [Source:MGI Symbol;Acc:MGI:99516]
Rftn1	ENSMUSG00000039316	raftlin lipid raft linker 1 [Source:MGI Symbol;Acc:MGI:1923688]

Table S1. Duodenum TRAP signature. Table of genes that are significantly enriched in the duodenum of *Snap25*$^{\text{RiboTag}}$ mice as compared to both the ileum and colon. Used as a filter to generate the volcano plots in Figure 2D.

Movie S1. AdipoClear whole-mount SPF ileum stained with anti-TUJ1.

Movie S2. AdipoClear whole-mount GF ileum stained with anti-TUJ1.

Movie S3. AdipoClear whole-mount SPF colon stained with anti-TUJ1.

Movie S4. AdipoClear whole-mount GF colon stained with anti-TUJ.

Movie S5. AdipoClear whole-mount *Cartpt*$^{EAN\text{-}hM3Dq}$ colon stained with anti-RFP.

References and Notes

1. E. A. Mayer, Gut feelings: The emerging biology of gut-brain communication. *Nat. Rev. Neurosci.* **12**, 453–466 (2011). doi:10.1038/nrn3071 Medline

2. J. B. Furness, L. R. Rivera, H. J. Cho, D. M. Bravo, B. Callaghan, The gut as a sensory organ. *Nat. Rev. Gastroenterol. Hepatol.* **10**, 729–740 (2013). doi:10.1038/nrgastro.2013.180 Medline

3. H. Veiga-Fernandes, D. Mucida, Neuro-immune interactions at barrier surfaces. *Cell* **165**, 801–811 (2016). doi:10.1016/j.cell.2016.04.041 Medline

4. V. K. Ridaura, J. J. Faith, F. E. Rey, J. Cheng, A. E. Duncan, A. L. Kau, N. W. Griffin, V. Lombard, B. Henrissat, J. R. Bain, M. J. Muehlbauer, O. Ilkayeva, C. F. Semenkovich, K. Funai, D. K. Hayashi, B. J. Lyle, M. C. Martini, L. K. Ursell, J. C. Clemente, W. Van Treuren, W. A. Walters, R. Knight, C. B. Newgard, A. C. Heath, J. I. Gordon, Gut microbiota from twins discordant for obesity modulate metabolism in mice. *Science* **341**, 1241214 (2013). doi:10.1126/science.1241214 Medline

5. P. A. Muller, M. Schneeberger, F. Matheis, P. Wang, Z. Kerner, A. Ilanges, K. Pellegrino, J. Del Mármol, T. B. R. Castro, M. Furuichi, M. Perkins, W. Han, A. Rao, A. J. Picard, J. R. Cross, K. Honda, I. de Araujo, D. Mucida, Microbiota modulate sympathetic neurons via a gut-brain circuit. *Nature* **583**, 441–446 (2020). doi:10.1038/s41586-020-2474-7 Medline

6. Q. Sang, H. M. Young, Chemical coding of neurons in the myenteric plexus and external muscle of the small and large intestine of the mouse. *Cell Tissue Res.* **284**, 39–53 (1996). doi:10.1007/s004410050565 Medline

7. F. M. Gribble, F. Reimann, Enteroendocrine cells: Chemosensors in the intestinal epithelium. *Annu. Rev. Physiol.* **78**, 277–299 (2016). doi:10.1146/annurev-physiol-021115-105439 Medline

8. D. H. Teitelbaum, T. M. O'Dorisio, W. E. Perkins, T. S. Gaginella, Somatostatin modulation of peptide-induced acetylcholine release in guinea pig ileum. *Am. J. Physiol.* **246**, G509–G514 (1984). Medline

9. E. Ekblad, M. Kuhar, N. Wierup, F. Sundler, Cocaine- and amphetamine-regulated transcript: Distribution and function in rat gastrointestinal tract. *Neurogastroenterol. Motil.* **15**, 545–557 (2003). doi:10.1046/j.1365-2982.2003.00437.x Medline

10. A. Lecci, M. Altamura, A. Capriati, C. A. Maggi, Tachykinin receptors and gastrointestinal motility: Focus on humans. *Eur. Rev. Med. Pharmacol. Sci.* **12** (suppl. 1), 69–80 (2008). Medline

11. P. Holzer, Opioid receptors in the gastrointestinal tract. *Regul. Pept.* **155**, 11–17 (2009). doi:10.1016/j.regpep.2009.03.012 Medline

12. L. P. Degen, F. Peng, A. Collet, L. Rossi, S. Ketterer, Y. Serrano, F. Larsen, C. Beglinger, P. Hildebrand, Blockade of GRP receptors inhibits gastric emptying and gallbladder contraction but accelerates small intestinal transit. *Gastroenterology* **120**, 361–368 (2001). doi:10.1053/gast.2001.21174 Medline

13. J. R. Grider, Neurotransmitters mediating the intestinal peristaltic reflex in the mouse. *J. Pharmacol. Exp. Ther.* **307**, 460–467 (2003). doi:10.1124/jpet.103.053512 Medline

14. K. N. Browning, G. M. Lees, Inhibitory effects of NPY on ganglionic transmission in myenteric neurones of the guinea-pig descending colon. *Neurogastroenterol. Motil.* **12**, 33–41 (2000). doi:10.1046/j.1365-2982.2000.00178.x Medline

15. O. J. Mace, B. Tehan, F. Marshall, Pharmacology and physiology of gastrointestinal enteroendocrine cells. *Pharmacol. Res. Perspect.* **3**, e00155 (2015). doi:10.1002/prp2.155 Medline

16. K. Makowska, L. Rytel, P. Lech, A. Osowski, E. Kruminis-Kaszkiel, S. Gonkowski, Cocaine- and amphetamine-regulated transcript (CART) peptide in the enteric nervous system of the porcine esophagus. *C. R. Biol.* **341**, 325–333 (2018). doi:10.1016/j.crvi.2018.06.006 Medline

17. K. Sonoyama, S. Rutatip, T. Kasai, Gene expression of activin, activin receptors, and follistatin in intestinal epithelial cells. *Am. J. Physiol. Gastrointest. Liver Physiol.* **278**, G89–G97 (2000). doi:10.1152/ajpgi.2000.278.1.G89 Medline

18. T. Byun, M. Karimi, J. L. Marsh, T. Milovanovic, F. Lin, R. F. Holcombe, Expression of secreted Wnt antagonists in gastrointestinal tissues: Potential role in stem cell homeostasis. *J. Clin. Pathol.* **58**, 515–519 (2005). doi:10.1136/jcp.2004.018598 Medline

19. V. Cardoso, J. Chesné, H. Ribeiro, B. García-Cassani, T. Carvalho, T. Bouchery, K. Shah, N. L. Barbosa-Morais, N. Harris, H. Veiga-Fernandes, Neuronal regulation of type 2 innate lymphoid cells via neuromedin U. *Nature* **549**, 277–281 (2017). doi:10.1038/nature23469 Medline

20. V. Lakhina, R. N. Arey, R. Kaletsky, A. Kauffman, G. Stein, W. Keyes, D. Xu, C. T. Murphy, Genome-wide functional analysis of CREB/long-term memory-dependent transcription reveals distinct basal and memory gene expression programs. *Neuron* **85**, 330–345 (2015). doi:10.1016/j.neuron.2014.12.029 Medline

21. K. A. McVey Neufeld, A. Perez-Burgos, Y. K. Mao, J. Bienenstock, W. A. Kunze, The gut microbiome restores intrinsic and extrinsic nerve function in germ-free mice accompanied by changes in calbindin. *Neurogastroenterol. Motil.* **27**, 627–636 (2015). doi:10.1111/nmo.12534 Medline

22. F. Matheis, P. A. Muller, C. L. Graves, I. Gabanyi, Z. J. Kerner, D. Costa-Borges, T. Ahrends, P. Rosenstiel, D. Mucida, Adrenergic signaling in muscularis macrophages limits infection-induced neuronal loss. *Cell* **180**, 64–78.e16 (2020). doi:10.1016/j.cell.2019.12.002 Medline

23. A. R. Gunawardene, B. M. Corfe, C. A. Staton, Classification and functions of enteroendocrine cells of the lower gastrointestinal tract. *Int. J. Exp. Pathol.* **92**, 219–231 (2011). doi:10.1111/j.1365-2613.2011.00767.x Medline

24. M. J. Waterson, T. L. Horvath, Neuronal regulation of energy homeostasis: Beyond the hypothalamus and feeding. *Cell Metab.* **22**, 962–970 (2015). doi:10.1016/j.cmet.2015.09.026 Medline

25. R. Gupta, Y. Ma, M. Wang, M. D. Whim, AgRP-expressing adrenal chromaffin cells are involved in the sympathetic response to fasting. *Endocrinology* **158**, 2572–2584 (2017). doi:10.1210/en.2016-1268 Medline

26. X. Yuan, Y. Huang, S. Shah, H. Wu, L. Gautron, Levels of cocaine- and amphetamine-regulated transcript in vagal afferents in the mouse are unaltered in response to metabolic challenges. *eNeuro* **3**, ENEURO.0174-16.2016 (2016). doi:10.1523/ENEURO.0174-16.2016 Medline

27. T. J. Hibberd, V. P. Zagorodnyuk, N. J. Spencer, S. J. Brookes, Identification and mechanosensitivity of viscerofugal neurons. *Neuroscience* **225**, 118–129 (2012). doi:10.1016/j.neuroscience.2012.08.040 Medline

28. J. Havrankova, J. Roth, M. Brownstein, Insulin receptors are widely distributed in the central nervous system of the rat. *Nature* **272**, 827–829 (1978). doi:10.1038/272827a0 Medline

29. J. A. Love, E. Yi, T. G. Smith, Autonomic pathways regulating pancreatic exocrine secretion. *Auton. Neurosci.* **133**, 19–34 (2007). doi:10.1016/j.autneu.2006.10.001 Medline

30. K. Mizuno, Y. Ueno, Autonomic nervous system and the liver. *Hepatol. Res.* **47**, 160–165 (2017). doi:10.1111/hepr.12760 Medline

31. A. Zarrinpar, A. Chaix, Z. Z. Xu, M. W. Chang, C. A. Marotz, A. Saghatelian, R. Knight, S. Panda, Antibiotic-induced microbiome depletion alters metabolic homeostasis by affecting gut signaling and colonic metabolism. *Nat. Commun.* **9**, 2872 (2018). doi:10.1038/s41467-018-05336-9 Medline

32. A. M. Martin, J. M. Yabut, J. M. Choo, A. J. Page, E. W. Sun, C. F. Jessup, S. L. Wesselingh, W. I. Khan, G. B. Rogers, G. R. Steinberg, D. J. Keating, The gut microbiome regulates host glucose homeostasis via peripheral serotonin. *Proc. Natl. Acad. Sci. U.S.A.* **116**, 19802–19804 (2019). doi:10.1073/pnas.1909311116 Medline

33. T. I. Krisko, H. T. Nicholls, C. J. Bare, C. D. Holman, G. G. Putzel, R. S. Jansen, N. Sun, K. Y. Rhee, A. S. Banks, D. E. Cohen, Dissociation of adaptive thermogenesis from glucose homeostasis in microbiome-deficient mice. *Cell Metab.* **31**, 592–604.e9 (2020). doi:10.1016/j.cmet.2020.01.012 Medline

34. T. Korem, D. Zeevi, N. Zmora, O. Weissbrod, N. Bar, M. Lotan-Pompan, T. Avnit-Sagi, N. Kosower, G. Malka, M. Rein, J. Suez, B. Z. Goldberg, A. Weinberger, A. A. Levy, E. Elinav, E. Segal, Bread affects clinical parameters and induces gut microbiome-associated personal glycemic responses. *Cell Metab.* **25**, 1243–1253.e5 (2017). doi:10.1016/j.cmet.2017.05.002 Medline

35. K. Honda, D. R. Littman, The microbiota in adaptive immune homeostasis and disease. *Nature* **535**, 75–84 (2016). doi:10.1038/nature18848 Medline

36. J. M. Yano, K. Yu, G. P. Donaldson, G. G. Shastri, P. Ann, L. Ma, C. R. Nagler, R. F. Ismagilov, S. K. Mazmanian, E. Y. Hsiao, Indigenous bacteria from the gut microbiota regulate host serotonin biosynthesis. *Cell* **161**, 264–276 (2015). doi:10.1016/j.cell.2015.02.047 Medline

37. S. Kim, H. Kim, Y. S. Yim, S. Ha, K. Atarashi, T. G. Tan, R. S. Longman, K. Honda, D. R. Littman, G. B. Choi, J. R. Huh, Maternal gut bacteria promote neurodevelopmental abnormalities in mouse offspring. *Nature* **549**, 528–532 (2017). doi:10.1038/nature23910 Medline

38. M. Levy, C. A. Thaiss, D. Zeevi, L. Dohnalová, G. Zilberman-Schapira, J. A. Mahdi, E. David, A. Savidor, T. Korem, Y. Herzig, M. Pevsner-Fischer, H. Shapiro, A. Christ, A. Harmelin, Z. Halpern, E. Latz, R. A. Flavell, I. Amit, E. Segal, E. Elinav, Microbiota-modulated metabolites shape the intestinal microenvironment by regulating NLRP6 inflammasome signaling. *Cell* **163**, 1428–1443 (2015). doi:10.1016/j.cell.2015.10.048 Medline

39. M. M. Kaelberer, K. L. Buchanan, M. E. Klein, B. B. Barth, M. M. Montoya, X. Shen, D. V. Bohórquez, A gut-brain neural circuit for nutrient sensory transduction. *Science* **361**, eaat5236 (2018). doi:10.1126/science.aat5236 Medline

40. W. Han, L. A. Tellez, M. H. Perkins, I. O. Perez, T. Qu, J. Ferreira, T. L. Ferreira, D. Quinn, Z.-W. Liu, X.-B. Gao, M. M. Kaelberer, D. V. Bohórquez, S. J. Shammah-Lagnado, G. de Lartigue, I. E. de Araujo, A neural circuit for gut-induced reward. *Cell* **175**, 665–678.e23 (2018). doi:10.1016/j.cell.2018.08.049 Medline

41. M. J. Benskey, N. C. Kuhn, J. J. Galligan, J. Garcia, S. E. Boye, W. W. Hauswirth, C. Mueller, S. L. Boye, F. P. Manfredsson, Targeted gene delivery to the enteric nervous system using AAV: A comparison across serotypes and capsid mutants. *Mol. Ther.* **23**, 488–500 (2015). doi:10.1038/mt.2015.7 Medline

42. M. J. Krashes, S. Koda, C. Ye, S. C. Rogan, A. C. Adams, D. S. Cusher, E. Maratos-Flier, B. L. Roth, B. B. Lowell, Rapid, reversible activation of AgRP neurons drives feeding behavior in mice. *J. Clin. Invest.* **121**, 1424–1428 (2011). doi:10.1172/JCI46229 Medline

43. Z. Wu, A. E. Autry, J. F. Bergan, M. Watabe-Uchida, C. G. Dulac, Galanin neurons in the medial preoptic area govern parental behaviour. *Nature* **509**, 325–330 (2014). doi:10.1038/nature13307 Medline

44. I. Gabanyi, P. A. Muller, L. Feighery, T. Y. Oliveira, F. A. Costa-Pinto, D. Mucida, Neuro-immune interactions drive tissue programming in intestinal macrophages. *Cell* **164**, 378–391 (2016). doi:10.1016/j.cell.2015.12.023 Medline

45. E. Sanz, L. Yang, T. Su, D. R. Morris, G. S. McKnight, P. S. Amieux, Cell-type-specific isolation of ribosome-associated mRNA from complex tissues. *Proc. Natl. Acad. Sci. U.S.A.* **106**, 13939–13944 (2009). doi:10.1073/pnas.0907143106 Medline

46. M. Heiman, R. Kulicke, R. J. Fenster, P. Greengard, N. Heintz, Cell type-specific mRNA purification by translating ribosome affinity purification (TRAP). *Nat. Protoc.* **9**, 1282–1291 (2014). doi:10.1038/nprot.2014.085 Medline

47. N. L. Bray, H. Pimentel, P. Melsted, L. Pachter, Near-optimal probabilistic RNA-seq quantification. *Nat. Biotechnol.* **34**, 525–527 (2016). doi:10.1038/nbt.3519 Medline

48. M. I. Love, W. Huber, S. Anders, Moderated estimation of fold change and dispersion for RNA-seq data with DESeq2. *Genome Biol.* **15**, 550 (2014). doi:10.1186/s13059-014-0550-8 Medline

49. B. N. Smith, B. W. Banfield, C. A. Smeraski, C. L. Wilcox, F. E. Dudek, L. W. Enquist, G. E. Pickard, Pseudorabies virus expressing enhanced green fluorescent protein: A tool for in vitro electrophysiological analysis of transsynaptically labeled neurons in identified central nervous system circuits. *Proc. Natl. Acad. Sci. U.S.A.* **97**, 9264–9269 (2000). doi:10.1073/pnas.97.16.9264 Medline

50. B. W. Banfield, J. D. Kaufman, J. A. Randall, G. E. Pickard, Development of pseudorabies virus strains expressing red fluorescent proteins: New tools for multisynaptic labeling applications. *J. Virol.* **77**, 10106–10112 (2003). doi:10.1128/JVI.77.18.10106-10112.2003 Medline

51. J. Chi, Z. Wu, C. H. J. Choi, L. Nguyen, S. Tegegne, S. E. Ackerman, A. Crane, F. Marchildon, M. Tessier-Lavigne, P. Cohen, Three-dimensional adipose tissue imaging reveals regional variation in beige fat biogenesis and PRDM16-dependent sympathetic neurite density. *Cell Metab.* **27**, 226–236.e3 (2018). doi:10.1016/j.cmet.2017.12.011 Medline